# A SECOND-ORDER IN TIME APPROXIMATION OF FLUID-STRUCTURE INTERACTION PROBLEM*

OYEKOLA OYEKOLE†, CATALIN TRENCHEA‡, AND MARTINA BUKAČ§

**Abstract.** We propose and analyze a novel, second-order in time, partitioned method for the interaction between an incompressible, viscous fluid and a thin, elastic structure. The proposed numerical method is based on the Crank–Nicolson discretization scheme, which is used to decouple the system into a fluid subproblem and a structure subproblem. The scheme is loosely coupled, and therefore at every time step, each subproblem is solved only once. Energy and error estimates for a fully discretized scheme using finite element spatial discretization are derived. We prove that the scheme is stable under a CFL condition, second-order convergent in time, and optimally convergent in space. Numerical examples support the theoretically obtained results and demonstrate the applicability of the method to realistic simulations of blood flow.

**Key words.** fluid-structure interaction, second-order scheme, partitioned scheme, finite element method, Crank–Nicolson

**AMS subject classifications.** Primary, 65M15, 74F10; Secondary, 65M60, 74S05, 74H15, 76M10

**DOI.** 10.1137/17M1140054

**1. Introduction.** Fluid-structure interaction (FSI) problems arise in many applications, such as aerodynamics, geomechanics, and biomedical engineering. They are characterized by highly nonlinear coupling between two different physical phenomena. As a result, the development of robust numerical algorithms is a subject of intensive research. Because coupled FSI problems give rise to large and ill-conditioned systems of algebraic equations, partitioned methods have often been used to split the coupled problem into smaller and better conditioned subproblems. However, in applications where the density of the structure is comparable to the density of the fluid, such as the interaction between blood and arterial walls, classical partitioned schemes suffer from instabilities known as *the added mass effect* [12]. In that case, the development of stable, noniterative numerical schemes for FSI problems is challenging even for first-order accurate solution techniques.

The stability of partitioned methods for FSI problems is highly sensitive to the way the interface coupling conditions are treated at the discrete level. A membrane model is used to describe the structure elastodynamics in [17, 23] and was embedded into the fluid problem as a generalized Robin boundary condition. A novel combination of coupling conditions was introduced in [2, 1], which gave rise to fluid and structure subproblems with Robin boundary conditions. Karniadakis and others [3, 26] proposed fictitious-pressure and fictitious-mass algorithms, in which the added mass

†Department of Applied and Computational Mathematics and Statistics, University of Notre Dame, South Bend, IN 46556 (ooyekole@nd.edu).

‡Department of Mathematics, University of Pittsburgh, Pittsburgh, PA 15260 (trenchea@pitt.edu).

§Corresponding author. Department of Applied and Computational Mathematics and Statistics, University of Notre Dame, South Bend, IN 46556 (mbukac@nd.edu).

effect is accounted for by incorporating additional terms into governing equations. However, algorithms proposed in [2, 1, 23, 3, 26] require subiterations between the fluid and the structure subproblems in order to achieve stability. A partitioned scheme based on the Nitsche's penalty method was proposed in [10, 11]. In order to obtain stability, a stabilization term was added to control the pressure variations at the interface. The splitting error, however, lowers the temporal accuracy of the scheme, which was then corrected by proposing a few defect-correction subiterations to achieve an optimal, first-order convergence rate.

Noniterative, partitioned numerical schemes based on the Lie operator splitting were proposed in [15, 9, 8]. The "incremental displacement–correction scheme" introduced in [15] is obtained by adding and subtracting the elastic operator applied to the displacement from the previous time step, while the "kinematically coupled $\beta$ scheme" introduced in [9, 8] is obtained by adding and subtracting the fluid pressure from the previous time step, resulting in a fluid subproblem solved with a Robin boundary condition which takes into account the mass of the structure at the fluid-structure interface. The incremental displacement–correction scheme and the kinematically coupled $\beta$ scheme for $\beta = 1$ have been shown to be first-order convergent in time [15, 8].

Due to the difficulties in deriving and analyzing second-order partitioned schemes for FSI problems, few methods are available in the literature. A second-order splitting approach based on the Strang splitting was proposed in [21, 20] to study the FSI involving non-Newtonian fluids. That method involves a solution of the structure subproblem, the fluid subproblem, and the structure subproblem once more, solving three subproblems within each time step. However, the order of convergence was only investigated in numerical experiments. Partitioned algorithms based on predictor-corrector method are proposed in [5, 4]. Following the predictor-corrector approach, they require a solution of the fluid subproblem and the structure sub-problem twice within one time step. The number of subproblems could be reduced since the corrector step is optional. However, the corrector step is recommended for accuracy reasons and to increase the region of stability. Using the von Neumann stability analysis, the authors showed that the algorithm proposed in [4] is stable under a condition on the time step which depends on the structure parameters, while the algorithm proposed in [5] is weakly stable under a Courant–Friedrichs–Lewy (CFL) condition. Although the numerical results indicate second-order convergence in time, the convergence rates are not analytically derived.

In this paper, we propose a novel, partitioned algorithm for FSI between an incompressible viscous fluid and a thin elastic structure. As oppose to the existing methods [21, 20, 5, 4], the fluid and solid subproblems are solved only once within each time step. We assume that the fluid is modeled using the Stokes equations and that the structure displacement is infinitesimal. The fluid and structure subproblems are discretized in time using the Crank–Nicolson method, and the decoupling of the two subproblems is based on the kinematically coupled $\beta$ scheme [8]. In order to achieve stability, the fluid problem is solved with a Robin boundary condition containing structure inertia at the fluid-structure interface. Since the splitting of the two subproblems often gives rise to suboptimal time convergence rates, fluid stress at time $t^{n-\frac{1}{2}}$ was added and subtracted to ensure second-order convergence in time. The stability and convergence of the fully discretized scheme is analyzed, where the discretization in space is performed using the finite element method. Energy estimates yield stability under a CFL condition. Based on the a priori error estimates, the scheme is second-order convergent in time and optimally convergent

in space. Two numerical examples are presented to support the analytical results. The first example numerically confirms the second-order convergence in time on a benchmark problem commonly used to verify FSI solvers with applications to hemodynamics. In this example, fluid is modeled using the Stokes equations and the structure is modeled using a generalized string model. The second numerical example consists of a study of blood flow in a common carotid artery. To model blood flow, we used the Navier–Stokes equations, while a linear membrane model was used to describe the structure displacement. Under realistic parameter values, our simulation results demonstrate that the proposed scheme is applicable to problems related to blood flow modeling, with the accuracy comparable to that obtained by an implicit scheme.

This paper is organized as follows. The linear FSI problem is presented in section 2, and the proposed numerical scheme is presented in section 3. Stability analysis is performed in section 4 and error analysis is performed in section 5. Numerical examples are presented in section 6. Conclusions are drawn in section 7.

**2. Description of the problem.** We consider an FSI problem in a low Reynolds number regime and assume that the structure undergoes infinitesimal displacements. Let $\Omega \subset \mathbb{R}^d$, $d = 2, 3$, be an open, smooth set and $\partial\Omega = \Gamma \cup \Gamma_{in} \cup \Gamma_{out}$, where $\Gamma$ represents elastic part of the boundary while $\Gamma_{in}$ and $\Gamma_{out}$ represent artificial inflow and outflow sections; see Figure 1. We assume that the fluid is incompressible, viscous, and Newtonian. Furthermore, we assume that the structure is described by some lower dimensional, linearly elastic model (for example, string, membrane, shell, etc). These assumptions give rise to a linear problem, which is commonly considered in the literature [15, 8]. For nonlinear, moving boundary FSI problems, even the existence of a solution is a challenging question [22].

We model the fluid using the time-dependent Stokes equations in a fixed domain $\Omega$,

$$(2.1) \qquad \rho_f \partial_t \boldsymbol{u} = \nabla \cdot \boldsymbol{\sigma}(\boldsymbol{u}, p), \qquad \nabla \cdot \boldsymbol{u} = 0 \qquad \text{in } \Omega \times (0, T),$$

$$(2.2) \qquad \boldsymbol{\sigma}(\boldsymbol{u}, p)\boldsymbol{n} = p_{in}(t)\boldsymbol{n} \qquad \text{on } \Gamma_{in} \times (0, T),$$

$$(2.3) \qquad \boldsymbol{\sigma}(\boldsymbol{u}, p)\boldsymbol{n} = p_{out}(t)\boldsymbol{n} \qquad \text{on } \Gamma_{out} \times (0, T),$$

$$(2.4) \qquad \boldsymbol{u}(., 0) = \boldsymbol{u}^0 \qquad \text{in } \Omega,$$

where $\boldsymbol{u} = (u_i)_{i=1,\dots,d}$ is the fluid velocity, $\boldsymbol{\sigma}(\boldsymbol{u}, p) = -p\boldsymbol{I} + 2\mu\boldsymbol{D}(\boldsymbol{u})$ is the fluid stress tensor, $\boldsymbol{D}(\boldsymbol{u}) = \frac{1}{2}(\nabla\boldsymbol{u} + (\nabla\boldsymbol{u})^T)$ is the strain rate tensor, $p$ is the fluid pressure, $\mu$ is the fluid viscosity, $\rho_f$ is the fluid density, $\boldsymbol{n}$ is the outward normal to the fluid boundary, and $p_{in}$ and $p_{out}$ are prescribed inflow and outflow forcing terms.
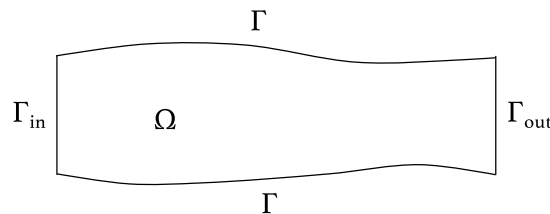


FIG. 1. *Fluid domain $\Omega$. The lateral boundary $\Gamma$ represents elastic structure.*

The structure elastodynamics are described using a linearly elastic model, given by

$$(2.5) \qquad \rho_s h \partial_{tt} \boldsymbol{\eta} + \mathcal{L}_e \boldsymbol{\eta} = \boldsymbol{f} \qquad\qquad \text{on } \Gamma \times (0, T),$$

$$(2.6) \qquad \boldsymbol{\eta} = 0 \qquad\qquad\qquad\qquad \text{on } \partial\Gamma \times (0, T),$$

$$(2.7) \qquad \boldsymbol{\eta}(.,0) = \boldsymbol{\eta}^0, \ \partial_t \boldsymbol{\eta}(.,0) = \boldsymbol{\eta}_v^0 \qquad\qquad \text{on } \Gamma,$$

where $\boldsymbol{\eta} = (\eta_i)_{i=1,...,d}$ denotes the structure displacement, $\boldsymbol{f}$ is a vector of surface density of the force applied to the thin structure, $\rho_s$ denotes the structure density, $h$ denotes the structure thickness, and the operator $\mathcal{L}_e$ describes the elastic behavior of the structure. Examples of such operators are the ones associated with the linearly elastic cylindrical Koiter shell used in [9] and the generalized string model used in [8]. Equation (2.6) accounts for clamped boundary conditions.

To couple the fluid and structure, we prescribe the following kinematic and dynamic interface conditions:

(2.8)
The continuity of velocity (kinematic condition): $\qquad\qquad \partial_t \boldsymbol{\eta} = \boldsymbol{u} \quad$ on $\Gamma \times (0, T),$

(2.9)
The balance of contact forces (dynamic condition): $\quad \boldsymbol{f} = -\boldsymbol{\sigma}(\boldsymbol{u}, p)\boldsymbol{n} \quad$ on $\Gamma \times (0, T).$

Taking into account the conditions (2.8)–(2.9), the coupled FSI problem can be written as

$$(2.10) \qquad \rho_f \partial_t \boldsymbol{u} = \nabla \cdot \boldsymbol{\sigma}(\boldsymbol{u}, p) \qquad\qquad \text{in } \Omega \times (0, T),$$

$$(2.11) \qquad \nabla \cdot \boldsymbol{u} = 0 \qquad\qquad\qquad\qquad \text{in } \Omega \times (0, T),$$

$$(2.12) \qquad \rho_s h \partial_t \boldsymbol{u} + \mathcal{L}_e \boldsymbol{\eta} = -\boldsymbol{\sigma}(\boldsymbol{u}, p)\boldsymbol{n} \qquad \text{on } \Gamma \times (0, T),$$

$$(2.13) \qquad \partial_t \boldsymbol{\eta} = \boldsymbol{u} \qquad\qquad\qquad\qquad \text{on } \Gamma \times (0, T)$$

with boundary conditions (2.2), (2.3), and (2.6).

**2.1. Preliminaries and monolithic weak formulation.** We consider the usual Sobolev spaces $H^k(S)$ with $k \geq 0$. We also use the closed subspace $H_0^1(S)$, consisting of functions in $H^1(S)$ with zero trace on $\partial S$. We introduce the following functional spaces:

$$V^f = (H^1(\Omega))^d, \quad Q = L^2(\Omega), \quad V^s = (H_0^1(\Gamma))^d, \quad V^{fsi} = \{(\boldsymbol{\varphi}, \boldsymbol{\zeta}) \in V^f \times V^s | \boldsymbol{\varphi}|_\Gamma = \boldsymbol{\zeta}\}.$$

We define the following bilinear forms associated with the fluid problem:

$$(2.14) \qquad a_f(\boldsymbol{u}, \boldsymbol{\varphi}) = 2\mu \int_\Omega \boldsymbol{D}(\boldsymbol{u}) : \boldsymbol{D}(\boldsymbol{\varphi}) d\boldsymbol{x}, \qquad b(p, \boldsymbol{\varphi}) = \int_\Omega p \nabla \cdot \boldsymbol{\varphi} d\boldsymbol{x}.$$

We denote by $a_e(\cdot, \cdot)$ the bilinear form associated with the structure operator $\mathcal{L}_e$, given by

$$(2.15) \qquad\qquad\qquad a_e(\boldsymbol{\eta}, \boldsymbol{\zeta}) = \int_\Gamma \mathcal{L}_e \boldsymbol{\eta} \cdot \boldsymbol{\zeta} dS.$$

We assume that $a_e$ is an inner-product into the space of admissible displacements (a subset of $(H_0^1(\Gamma))^d$) and set

$$(2.16) \qquad\qquad\qquad \|\boldsymbol{\eta}\|_E^2 = a_e(\boldsymbol{\eta}, \boldsymbol{\eta}).$$

Similar to [15] and [8], we assume that the $\| \cdot \|_E^2$ is equivalent to the $H^1(\Gamma)$-norm and there exists $\beta > 0$ such that the following continuity estimate holds:

$$\|\boldsymbol{\eta}\|_E^2 \leq \beta \|\boldsymbol{\eta}\|_{H^1(\Gamma)}^2 \quad \forall \boldsymbol{\eta} \in V^s. \tag{2.17}$$

The variational formulation of the monolithic FSI problem now reads as follows: given $t \in (0, T)$ find $(\boldsymbol{u}, \boldsymbol{\eta}, p) \in V^f \times V^s \times Q$ with $\boldsymbol{u} = \partial_t \boldsymbol{\eta}$ on $\Gamma$ such that for all $(\boldsymbol{\varphi}, \boldsymbol{\zeta}, q) \in V^{fsi} \times Q$ we have

$$\rho_f \int_\Omega \partial_t \boldsymbol{u} \cdot \boldsymbol{\varphi} dx + a_f(\boldsymbol{u}, \boldsymbol{\varphi}) - b(p, \boldsymbol{\varphi}) + b(q, \boldsymbol{u}) + \rho_s h \int_\Gamma \partial_{tt} \boldsymbol{\eta} \cdot \boldsymbol{\zeta} dx + a_e(\boldsymbol{\eta}, \boldsymbol{\zeta})$$
$$= \int_{\Gamma_{in}} p_{in} \boldsymbol{\varphi} \cdot \boldsymbol{n} dS + \int_{\Gamma_{out}} p_{out} \boldsymbol{\varphi} \cdot \boldsymbol{n} dS. \tag{2.18}$$

To derive an energy equality of the monolithic problem, let $(\boldsymbol{\varphi}, \boldsymbol{\zeta}, q) = (\boldsymbol{u}, \partial_t \boldsymbol{\eta}, p)$. Integrating from 0 to $T$, for $T > 0$, we have

$$\underbrace{\frac{\rho_f}{2} \|\boldsymbol{u}(T)\|_{L^2(\Omega)}^2 + \frac{\rho_s h}{2} \|\partial_t \boldsymbol{\eta}(T)\|_{L^2(\Gamma)}^2}_{\text{kinetic energy}} + \underbrace{\frac{1}{2} \|\boldsymbol{\eta}(T)\|_E^2}_{\text{elastic energy}} + \underbrace{2\mu \int_0^T \|\boldsymbol{D}(\boldsymbol{u})\|_{L^2(\Omega)}^2 dt}_{\text{viscous dissipation rate}}$$

$$= \frac{\rho_f}{2} \|\boldsymbol{u}(0)\|_{L^2(\Omega)}^2 + \frac{\rho_s h}{2} \|\partial_t \boldsymbol{\eta}(0)\|_{L^2(\Gamma)}^2$$
$$+ \frac{1}{2} \|\boldsymbol{\eta}(0)\|_E^2 + \int_0^T \int_{\Gamma_{in}} p_{in} \boldsymbol{\varphi} \cdot \boldsymbol{n} dS dt + \int_0^T \int_{\Gamma_{out}} p_{out} \boldsymbol{\varphi} \cdot \boldsymbol{n} dS dt. \tag{2.19}$$

**3. Crank–Nicolson FSI numerical scheme.** Let $t^n = n\Delta t$ for $n = 1, \ldots, N$, where $T = N\Delta t$ is the final time. We introduce the following notation:

$$\boldsymbol{\varphi}^{n+\frac{1}{2}} = \frac{\boldsymbol{\varphi}^{n+1} + \boldsymbol{\varphi}^n}{2} \quad \text{and} \quad d_t \boldsymbol{\varphi}^{n+1} = \frac{\boldsymbol{\varphi}^{n+1} - \boldsymbol{\varphi}^n}{\Delta t}. \tag{3.1}$$

We start by rewriting the structure equation (2.5) by taking into account the coupling conditions (2.8)–(2.9) as follows:

$$\rho_s h \partial_t \boldsymbol{u} + \mathcal{L}_e \boldsymbol{\eta} = -\boldsymbol{\sigma}(\boldsymbol{u}, p)\boldsymbol{n}. \tag{3.2}$$

We introduce the structure velocity $\boldsymbol{v} = \partial_t \boldsymbol{\eta}$ and discretize (3.2) using the Crank–Nicolson method (CNFSI). Similar to [8], we add and subtract the fluid normal stress at time $t^{n-\frac{1}{2}}$ and split (3.2) using operator splitting into the following two equations:

$$\rho_s h \frac{\boldsymbol{v}^{n+1} - \boldsymbol{u}^n}{\Delta t} + \mathcal{L}_e \boldsymbol{\eta}^{n+\frac{1}{2}} = -\boldsymbol{\sigma}\left(\boldsymbol{u}^{n-\frac{1}{2}}, p^{n-\frac{1}{2}}\right)\boldsymbol{n}, \tag{3.3}$$

$$\rho_s h \frac{\boldsymbol{u}^{n+1} - \boldsymbol{v}^{n+1}}{\Delta t} = -\boldsymbol{\sigma}\left(\boldsymbol{u}^{n+\frac{1}{2}}, p^{n+\frac{1}{2}}\right)\boldsymbol{n} + \boldsymbol{\sigma}\left(\boldsymbol{u}^{n-\frac{1}{2}}, p^{n-\frac{1}{2}}\right)\boldsymbol{n}. \tag{3.4}$$

The rest of the FSI problem (2.1)–(2.9) is discretized using the Crank–Nicolson method. Equation (3.3) is used to describe structure elastodynamics in the structure sub-problem and (3.4) is used as a Robin boundary condition in the fluid sub-problem as follows.

*CNFSI Step* 1 (solid subproblem). Given $t^{n+1} \in (0, T]$, $n = 0, \ldots, N - 1$, find $\boldsymbol{\eta}^{n+1}$ and $\boldsymbol{v}^{n+1}$ such that

$$d_t \boldsymbol{\eta}^{n+1} - \frac{\boldsymbol{v}^{n+1} + \boldsymbol{u}^n}{2} = 0 \qquad \qquad \text{on } \Gamma, \tag{3.5}$$

(3.6)     $\rho_s h \dfrac{\boldsymbol{v}^{n+1} - \boldsymbol{u}^n}{\Delta t} + \mathcal{L}_e \boldsymbol{\eta}^{n+\frac{1}{2}} = -\boldsymbol{\sigma}\left(\boldsymbol{u}^{n-\frac{1}{2}}, p^{n-\frac{1}{2}}\right)\boldsymbol{n}$     on $\Gamma$,

(3.7)     $\boldsymbol{\eta}^{n+1} = 0$     on $\partial\Gamma$.

*CNFSI Step* 2 (fluid subproblem). Find $\boldsymbol{u}^{n+1}$ and $p^{n+1}$ such that

(3.8)     $\rho_f d_t \boldsymbol{u}^{n+1} = \nabla \cdot \boldsymbol{\sigma}\left(\boldsymbol{u}^{n+\frac{1}{2}}, p^{n+\frac{1}{2}}\right)$     in $\Omega$,

(3.9)     $\nabla \cdot \boldsymbol{u}^{n+1} = 0$     in $\Omega$,

(3.10)    $\rho_s h \dfrac{\boldsymbol{u}^{n+1} - \boldsymbol{v}^{n+1}}{\Delta t} = -\boldsymbol{\sigma}\left(\boldsymbol{u}^{n+\frac{1}{2}}, p^{n+\frac{1}{2}}\right)\boldsymbol{n} + \boldsymbol{\sigma}\left(\boldsymbol{u}^{n-\frac{1}{2}}, p^{n-\frac{1}{2}}\right)\boldsymbol{n}$     on $\Gamma$,

(3.11)    $\boldsymbol{\sigma}(\boldsymbol{u}^{n+\frac{1}{2}}, p^{n+\frac{1}{2}})\boldsymbol{n} = p_{in}^{n+\frac{1}{2}}\boldsymbol{n}$     on $\Gamma_{in}$,

(3.12)    $\boldsymbol{\sigma}(\boldsymbol{u}^{n+\frac{1}{2}}, p^{n+\frac{1}{2}})\boldsymbol{n} = p_{out}^{n+\frac{1}{2}}\boldsymbol{n}$     on $\Gamma_{out}$.

In order to prescribe the additional initial conditions needed at the first time step, we define $\boldsymbol{u}^{-\frac{1}{2}} = 0, p^{-\frac{1}{2}} = 0$.

*Remark* 3.1. We note that the no-slip condition $\boldsymbol{u} = \boldsymbol{v}$ on $\Gamma$ is not exactly satisfied but is approximated to the second order of accuracy. In particular, from (3.10) we have

(3.13)     $\boldsymbol{u}^{n+1} - \boldsymbol{v}^{n+1} = \dfrac{\Delta t}{\rho_s h}\left(-\boldsymbol{\sigma}\left(\boldsymbol{u}^{n+\frac{1}{2}}, p^{n+\frac{1}{2}}\right)\boldsymbol{n} + \boldsymbol{\sigma}\left(\boldsymbol{u}^{n-\frac{1}{2}}, p^{n-\frac{1}{2}}\right)\boldsymbol{n}\right).$

Because $-\boldsymbol{\sigma}\left(\boldsymbol{u}^{n+\frac{1}{2}}, p^{n+\frac{1}{2}}\right)\boldsymbol{n} + \boldsymbol{\sigma}\left(\boldsymbol{u}^{n-\frac{1}{2}}, p^{n-\frac{1}{2}}\right)\boldsymbol{n} = -\frac{1}{2}\boldsymbol{\sigma}\left(\boldsymbol{u}^{n+1} - \boldsymbol{u}^{n-1}, p^{n+1} - p^{n-1}\right)\boldsymbol{n}$, we have

(3.14)                         $\boldsymbol{u}^{n+1} = \boldsymbol{v}^{n+1} + \mathcal{O}(\Delta t^2).$

To discretize the problem in space, we use the finite element method based on a conforming finite element triangulation with maximum triangle diameter $\Delta x$. We introduce the finite element spaces $V_h^f \subset V^f, Q_h \subset Q$, and $V_h^s \subset V^s$. The variational formulation of the fully discrete numerical scheme is given as follows.

*CNFSI Step* 1 (solid subproblem). Given $t^{n+1} \in (0, T]$, $n = 0, \ldots, N-1$, and $\boldsymbol{u}_h^{n-\frac{1}{2}}$ and $p_h^{n-\frac{1}{2}}$, find $\boldsymbol{v}_h^{n+1} \in V_h^s$ and $\boldsymbol{\eta}_h^{n+1} \in V_h^s$ such that for all $\boldsymbol{\zeta}_h \in V_h^s$ and $\boldsymbol{\chi}_h \in V_h^s$ we have

$$\rho_s h \int_\Gamma \frac{\boldsymbol{v}_h^{n+1} - \boldsymbol{u}_h^n}{\Delta t} \cdot \boldsymbol{\zeta}_h dS + a_e\left(\boldsymbol{\eta}_h^{n+\frac{1}{2}}, \boldsymbol{\zeta}_h\right) + \int_\Gamma d_t \boldsymbol{\eta}_h^{n+1} \cdot \boldsymbol{\chi}_h dS - \int_\Gamma \frac{\boldsymbol{v}_h^{n+1} + \boldsymbol{u}_h^n}{2} \cdot \boldsymbol{\chi}_h dS$$

$$= -\int_\Gamma \boldsymbol{\sigma}\left(\boldsymbol{u}_h^{n-\frac{1}{2}}, p_h^{n-\frac{1}{2}}\right)\boldsymbol{n} \cdot \boldsymbol{\zeta}_h dS.$$

(3.15)

*CNFSI Step* 2 (fluid subproblem). Given $\boldsymbol{v}_h^{n+1}$ computed in Step 1, find $\boldsymbol{u}_h^{n+1} \in V_h^f$ and $p_h^{n+1} \in Q_h$ such that for all $\boldsymbol{\varphi}_h \in V_h^f$ and $q_h \in Q_h$ we have

$$\rho_f \int_\Omega d_t \boldsymbol{u}_h^{n+1} \cdot \boldsymbol{\varphi}_h d\boldsymbol{x} + a_f\left(\boldsymbol{u}_h^{n+\frac{1}{2}}, \boldsymbol{\varphi}_h\right) - b\left(p_h^{n+\frac{1}{2}}, \boldsymbol{\varphi}_h\right)$$

$$+ b(q_h, \boldsymbol{u}_h^{n+1}) + \rho_s h \int_\Gamma \frac{\boldsymbol{u}_h^{n+1} - \boldsymbol{v}_h^{n+1}}{\Delta t} \cdot \boldsymbol{\varphi}_h dS$$

(3.16)   $= \int_\Gamma \boldsymbol{\sigma}\left(\boldsymbol{u}_h^{n-\frac{1}{2}}, p_h^{n-\frac{1}{2}}\right)\boldsymbol{n} \cdot \boldsymbol{\varphi}_h dS + \int_{\Gamma_{in}} p_{in}^{n+\frac{1}{2}}\boldsymbol{\varphi}_h \cdot \boldsymbol{n} dS + \int_{\Gamma_{out}} p_{out}^{n+\frac{1}{2}}\boldsymbol{\varphi}_h \cdot \boldsymbol{n} dS.$

**4. Stability analysis.** In this section we analyze the stability of the fully discrete CNFSI scheme (3.15)–(3.16). We first recall a version of the discrete Gronwall lemma [19] that is used in the analysis.

LEMMA 4.1 (a discrete Gronwall inequality [19]). *Let $\Delta t$, $B$, $a_N$, $b_N, c_N$, and $\gamma_N$ (for integers $N \geq 1$) be nonnegative numbers such that*

$$a_N + \Delta t \sum_{n=1}^{N} b_n \leq \Delta t \sum_{n=1}^{N} \gamma_n a_n + \Delta t \sum_{n=1}^{N} c_n + B \quad for\ N \geq 1.$$

*Suppose that $\Delta t \gamma_n < 1$ for all $n \geq 1$. Then, the following holds:*

$$a_N + \Delta t \sum_{n=1}^{N} b_n \leq \exp\left(\Delta t \sum_{n=1}^{N} \frac{\gamma_n}{1 - \Delta t \gamma_n}\right)\left(\Delta t \sum_{n=1}^{N} c_n + B\right) \quad for\ N \geq 1.$$

Furthermore, we assume that the solid operator $\mathcal{L}_e$ satisfies the following standard properties.

LEMMA 4.2. *For all $\boldsymbol{\eta}_h \in V_h^s$, we have [15]*

$$\tag{4.1} \|\boldsymbol{\eta}_h\|_E \leq \frac{\beta^{\frac{1}{2}} C_{inv}}{\Delta x} \|\boldsymbol{\eta}_h\|_{L^2(\Gamma)},$$

$$\tag{4.2} \|\mathcal{L}_e \boldsymbol{\eta}_h\|_{L^2(\Gamma)} \leq \frac{\beta^{\frac{1}{2}} C_{inv}}{\Delta x} \|\boldsymbol{\eta}_h\|_E,$$

*where $C_{inv} > 0$ is the constant of an inverse estimate.*

The stability of the CNFSI scheme is presented in the following theorem.

THEOREM 4.3. *Assume that the system is isolated, i.e., $p_{in} = p_{out} = 0$. Let $(\boldsymbol{v}_h^n, \boldsymbol{\eta}_h^n, \boldsymbol{u}_h^n, p_h^n)$ be the solution of (3.15)–(3.16). Assume that*

$$\tag{4.3} \Delta t < \frac{\sqrt{\rho_s h}}{\beta^{\frac{1}{2}} C_{inv}} \Delta x.$$

*Then, the following a priori energy estimate holds:*

$$\tag{4.4} \quad \mathcal{E}^N + \mathcal{D}^N + \mathcal{N}^N \leq \exp\left(\frac{T \beta C_{inv}^2 \Delta t}{\rho_s h \Delta x^2 - \beta C_{inv}^2 \Delta t^2}\right)\left(\mathcal{E}^0 + \frac{\mu \Delta t}{2} \left\|\boldsymbol{D}(\boldsymbol{u}_h^0)\right\|_{L^2(\Omega)}^2\right),$$

*where $\mathcal{E}^N$ is the sum of the kinetic energy of the fluid, kinetic energy of the structure and elastic energy of the structure*

$$\mathcal{E}^N = \frac{\rho_f}{2}\|\boldsymbol{u}_h^N\|_{L^2(\Omega)}^2 + \frac{\rho_s h}{2}\|\boldsymbol{u}_h^N\|_{L^2(\Gamma)}^2 + \frac{1}{2}\|\boldsymbol{\eta}_h^N\|_E^2,$$

$\mathcal{D}^N$ *is the fluid viscous dissipation rate*

$$\mathcal{D}^N = 2\mu \Delta t \sum_{n=0}^{N-1} \left\|\boldsymbol{D}(\boldsymbol{u}_h^{n+\frac{1}{2}})\right\|_{L^2(\Omega)}^2,$$

*and $\mathcal{N}^N$ denotes terms due to numerical dissipation*

$$\mathcal{N}^N = \frac{\mu \Delta t}{2} \left\|\boldsymbol{D}(\boldsymbol{u}_h^N)\right\|_{L^2(\Omega)}^2 + \frac{\Delta t^2}{2\rho_s h} \left\|\boldsymbol{\sigma}\left(\boldsymbol{u}_h^{N-\frac{1}{2}}, p_h^{N-\frac{1}{2}}\right)\boldsymbol{n}\right\|_{L^2(\Gamma)}^2$$

$$+ \frac{\rho_f}{2} \sum_{n=0}^{N-1} \left\|\boldsymbol{u}_h^{n+1} - \boldsymbol{u}_h^n\right\|_{L^2(\Omega)}^2 + \frac{\rho_s h}{3} \sum_{n=0}^{N-1} \left\|\boldsymbol{v}_h^{n+1} - \boldsymbol{u}_h^n\right\|_{L^2(\Gamma)}^2$$

$$+ \frac{\Delta t \delta}{8} \sum_{n=0}^{N-1} \left\|\boldsymbol{\eta}_h^{n+1} - \boldsymbol{\eta}_h^n\right\|_E^2 + \frac{\Delta t}{2} \sum_{n=0}^{N-1} \left\|\sqrt{\delta}\boldsymbol{\eta}_h^{n+\frac{1}{2}} - \frac{1}{\sqrt{\delta}}\frac{\boldsymbol{v}^{n+1} - \boldsymbol{u}^n}{2}\right\|_E^2.$$

*Proof.* We test (3.15) with $(\boldsymbol{\zeta}_h, \boldsymbol{\chi}_h) = (\boldsymbol{v}_h^{n+1}, \mathcal{L}_e \boldsymbol{\eta}_h^{n+\frac{1}{2}})$, test (3.16) with $(\boldsymbol{\varphi}_h, q_h) = (\boldsymbol{u}_h^{n+1}, p_h^{n+\frac{1}{2}})$, multiply by $\Delta t$, and add the equations together. Using the identity $a(a-b) = \frac{1}{2}a^2 - \frac{1}{2}b^2 + \frac{1}{2}(a-b)^2$, we obtain

$$\frac{\rho_s h}{2} \left( \|\boldsymbol{v}_h^{n+1}\|_{L^2(\Gamma)}^2 - \|\boldsymbol{u}_h^n\|_{L^2(\Gamma)}^2 + \|\boldsymbol{v}_h^{n+1} - \boldsymbol{u}_h^n\|_{L^2(\Gamma)}^2 \right) + \frac{1}{2} \left( \|\boldsymbol{\eta}_h^{n+1}\|_E^2 - \|\boldsymbol{\eta}_h^n\|_E^2 \right)$$

$$+ \frac{\rho_f}{2} \left( \|\boldsymbol{u}_h^{n+1}\|_{L^2(\Omega)}^2 - \|\boldsymbol{u}_h^n\|_{L^2(\Omega)}^2 \right) + \frac{\rho_f}{2} \|\boldsymbol{u}_h^{n+1} - \boldsymbol{u}_h^n\|_{L^2(\Omega)}^2$$

$$+ \frac{\mu \Delta t}{2} \left( \|\boldsymbol{D}(\boldsymbol{u}_h^{n+1})\|_{L^2(\Omega)}^2 - \|\boldsymbol{D}(\boldsymbol{u}_h^n)\|_{L^2(\Omega)}^2 + \|\boldsymbol{D}(\boldsymbol{u}_h^{n+1} + \boldsymbol{u}_h^n)\|_{L^2(\Omega)}^2 \right)$$

$$+ \frac{\rho_s h}{2} \left( \|\boldsymbol{u}_h^{n+1}\|_{L^2(\Gamma)}^2 - \|\boldsymbol{v}_h^{n+1}\|_{L^2(\Gamma)}^2 + \|\boldsymbol{u}_h^{n+1} - \boldsymbol{v}_h^{n+1}\|_{L^2(\Gamma)}^2 \right)$$

$$= \underbrace{\Delta t \int_\Gamma \boldsymbol{\sigma} \left( \boldsymbol{u}_h^{n-\frac{1}{2}}, p_h^{n-\frac{1}{2}} \right) \boldsymbol{n} \cdot (\boldsymbol{u}_h^{n+1} - \boldsymbol{v}_h^{n+1}) \, dS}_{\mathcal{I}_1}$$

$$+ \underbrace{\Delta t a_e \left( \boldsymbol{\eta}_h^{n+\frac{1}{2}}, \boldsymbol{v}^{n+1} \right) - \Delta t a_e \left( \boldsymbol{\eta}_h^{n+\frac{1}{2}}, \frac{\boldsymbol{v}^{n+1} + \boldsymbol{u}^n}{2} \right)}_{\mathcal{I}_2}.$$

(4.5)

Using (3.13), integral $\mathcal{I}_1$ becomes

$$\mathcal{I}_1 = \frac{\Delta t^2}{\rho_s h} \int_\Gamma \boldsymbol{\sigma} \left( \boldsymbol{u}_h^{n-\frac{1}{2}}, p_h^{n-\frac{1}{2}} \right) \boldsymbol{n} \cdot \left( \boldsymbol{\sigma} \left( \boldsymbol{u}_h^{n-\frac{1}{2}}, p_h^{n-\frac{1}{2}} \right) \boldsymbol{n} - \boldsymbol{\sigma} \left( \boldsymbol{u}_h^{n+\frac{1}{2}}, p_h^{n+\frac{1}{2}} \right) \boldsymbol{n} \right) dS$$

$$= \frac{\Delta t^2}{2\rho_s h} \left( \left\| \boldsymbol{\sigma} \left( \boldsymbol{u}_h^{n-\frac{1}{2}}, p_h^{n-\frac{1}{2}} \right) \boldsymbol{n} \right\|_{L^2(\Gamma)}^2 - \left\| \boldsymbol{\sigma} \left( \boldsymbol{u}_h^{n+\frac{1}{2}}, p_h^{n+\frac{1}{2}} \right) \boldsymbol{n} \right\|_{L^2(\Gamma)}^2 \right)$$

$$+ \frac{\Delta t^2}{2\rho_s h} \left\| \boldsymbol{\sigma} \left( \boldsymbol{u}_h^{n-\frac{1}{2}}, p_h^{n-\frac{1}{2}} \right) \boldsymbol{n} - \boldsymbol{\sigma} \left( \boldsymbol{u}_h^{n+\frac{1}{2}}, p_h^{n+\frac{1}{2}} \right) \boldsymbol{n} \right\|_{L^2(\Gamma)}^2.$$

Using (3.13) again, we have

$$(4.6) \qquad \mathcal{I}_1 = \frac{\Delta t^2}{2\rho_s h} \left( \left\| \boldsymbol{\sigma} \left( \boldsymbol{u}_h^{n-\frac{1}{2}}, p_h^{n-\frac{1}{2}} \right) \boldsymbol{n} \right\|_{L^2(\Gamma)}^2 - \left\| \boldsymbol{\sigma} \left( \boldsymbol{u}_h^{n+\frac{1}{2}}, p_h^{n+\frac{1}{2}} \right) \boldsymbol{n} \right\|_{L^2(\Gamma)}^2 \right)$$

$$+ \frac{\rho_s h}{2} \left\| \boldsymbol{u}_h^{n+1} - \boldsymbol{v}_h^{n+1} \right\|_{L^2(\Gamma)}^2.$$

To estimate integral $\mathcal{I}_2$, note that the following equality holds for $\delta > 0$:

$$\mathcal{I}_2 = \Delta t a_e \left( \boldsymbol{\eta}_h^{n+\frac{1}{2}}, \frac{\boldsymbol{v}_h^{n+1} - \boldsymbol{u}_h^n}{2} \right) = \frac{\Delta t \delta}{2} \left\| \boldsymbol{\eta}_h^{n+\frac{1}{2}} \right\|_E^2 + \frac{\Delta t}{2\delta} \left\| \frac{\boldsymbol{v}_h^{n+1} - \boldsymbol{u}_h^n}{2} \right\|_E^2$$

$$- \frac{\Delta t}{2} \left\| \sqrt{\delta} \boldsymbol{\eta}_h^{n+\frac{1}{2}} - \frac{1}{\sqrt{\delta}} \frac{\boldsymbol{v}_h^{n+1} - \boldsymbol{u}_h^n}{2} \right\|_E^2.$$

Using identity $(a+b)^2 = 2(a^2 + b^2) - (a-b)^2$, we can write

(4.7)
$$\frac{\Delta t \delta}{2} \left\| \boldsymbol{\eta}_h^{n+\frac{1}{2}} \right\|_E^2 = \frac{\Delta t \delta}{8} \left\| \boldsymbol{\eta}_h^{n+1} + \boldsymbol{\eta}_h^n \right\|_E^2 = \frac{\Delta t \delta}{4} \left( \left\| \boldsymbol{\eta}_h^{n+1} \right\|_E^2 + \left\| \boldsymbol{\eta}_h^n \right\|_E^2 \right) - \frac{\Delta t \delta}{8} \left\| \boldsymbol{\eta}_h^{n+1} - \boldsymbol{\eta}_h^n \right\|_E^2.$$

Taking into account (4.7), $\mathcal{I}_2$ becomes

$$\mathcal{I}_2 = \frac{\Delta t \delta}{4} \left( \left\| \boldsymbol{\eta}_h^{n+1} \right\|_E^2 + \left\| \boldsymbol{\eta}_h^n \right\|_E^2 \right) - \frac{\Delta t \delta}{8} \left\| \boldsymbol{\eta}_h^{n+1} - \boldsymbol{\eta}_h^n \right\|_E^2 + \frac{\Delta t}{2\delta} \left\| \frac{\boldsymbol{v}_h^{n+1} - \boldsymbol{u}_h^n}{2} \right\|_E^2$$

(4.8)
$$- \frac{\Delta t}{2} \left\| \sqrt{\delta} \boldsymbol{\eta}_h^{n+\frac{1}{2}} - \frac{1}{\sqrt{\delta}} \frac{\boldsymbol{v}_h^{n+1} - \boldsymbol{u}_h^n}{2} \right\|_E^2.$$

Combining (4.6) and (4.8) with (4.5) and summing from $n = 0$ to $N - 1$ we obtain

$$\frac{\rho_f}{2} \|\boldsymbol{u}_h^N\|_{L^2(\Omega)}^2 + \frac{\rho_s h}{2} \|\boldsymbol{u}_h^N\|_{L^2(\Gamma)}^2 + \frac{1}{2} \|\boldsymbol{\eta}_h^N\|_E^2 + \frac{\mu \Delta t}{2} \left\| \boldsymbol{D}(\boldsymbol{u}_h^N) \right\|_{L^2(\Omega)}^2$$

$$+ \frac{\Delta t^2}{2\rho_s h} \left\| \boldsymbol{\sigma} \left( \boldsymbol{u}_h^{N-\frac{1}{2}}, p_h^{N-\frac{1}{2}} \right) \boldsymbol{n} \right\|_{L^2(\Gamma)}^2 + \frac{\rho_f}{2} \sum_{n=0}^{N-1} \left\| \boldsymbol{u}_h^{n+1} - \boldsymbol{u}_h^n \right\|_{L^2(\Omega)}^2$$

$$+ 2\mu \Delta t \sum_{n=0}^{N-1} \left\| \boldsymbol{D}(\boldsymbol{u}_h^{n+\frac{1}{2}}) \right\|_{L^2(\Omega)}^2 + \frac{\rho_s h}{2} \sum_{n=0}^{N-1} \left\| \boldsymbol{v}_h^{n+1} - \boldsymbol{u}_h^n \right\|_{L^2(\Gamma)}^2$$

$$+ \frac{\Delta t \delta}{8} \sum_{n=0}^{N-1} \left\| \boldsymbol{\eta}_h^{n+1} - \boldsymbol{\eta}_h^n \right\|_E^2 + \frac{\Delta t}{2} \sum_{n=0}^{N-1} \left\| \sqrt{\delta} \boldsymbol{\eta}_h^{n+\frac{1}{2}} - \frac{1}{\sqrt{\delta}} \frac{\boldsymbol{v}_h^{n+1} - \boldsymbol{u}_h^n}{2} \right\|_E^2$$

$$= \frac{\rho_f}{2} \|\boldsymbol{u}_h^0\|_{L^2(\Omega)}^2 + \frac{\rho_s h}{2} \|\boldsymbol{u}_h^0\|_{L^2(\Gamma)}^2 + \frac{1}{2} \|\boldsymbol{\eta}_h^0\|_E^2 + \frac{\mu \Delta t}{2} \left\| \boldsymbol{D}(\boldsymbol{u}_h^0) \right\|_{L^2(\Omega)}^2$$

$$+ \frac{\delta \Delta t}{2} \sum_{n=0}^{N} \|\boldsymbol{\eta}_h^n\|_E^2 + \frac{\Delta t}{8\delta} \sum_{n=0}^{N-1} \left\| \boldsymbol{v}_h^{n+1} - \boldsymbol{u}_h^n \right\|_E^2.$$

Let $\delta = \frac{\beta C_{inv}^2 \Delta t}{\rho_s h \Delta x^2}$. Using (4.1) and Lemma 4.1 with $\gamma_n = \delta$, we have

$$\frac{\rho_f}{2} \|\boldsymbol{u}_h^N\|_{L^2(\Omega)}^2 + \frac{\rho_s h}{2} \|\boldsymbol{u}_h^N\|_{L^2(\Gamma)}^2 + \frac{1}{2} \|\boldsymbol{\eta}_h^N\|_E^2 + \frac{\mu \Delta t}{2} \left\| \boldsymbol{D}(\boldsymbol{u}_h^N) \right\|_{L^2(\Omega)}^2$$

$$+ \frac{\Delta t^2}{2\rho_s h} \left\| \boldsymbol{\sigma} \left( \boldsymbol{u}_h^{N-\frac{1}{2}}, p_h^{N-\frac{1}{2}} \right) \boldsymbol{n} \right\|_{L^2(\Gamma)}^2 + \frac{\rho_f}{2} \sum_{n=0}^{N-1} \left\| \boldsymbol{u}_h^{n+1} - \boldsymbol{u}_h^n \right\|_{L^2(\Omega)}^2$$

$$+ 2\mu \Delta t \sum_{n=0}^{N-1} \left\| \boldsymbol{D}(\boldsymbol{u}_h^{n+\frac{1}{2}}) \right\|_{L^2(\Omega)}^2 + \frac{3\rho_s h}{8} \sum_{n=0}^{N-1} \left\| \boldsymbol{v}_h^{n+1} - \boldsymbol{u}_h^n \right\|_{L^2(\Gamma)}^2 + \frac{\Delta t \delta}{8} \sum_{n=0}^{N-1} \left\| \boldsymbol{\eta}_h^{n+1} - \boldsymbol{\eta}_h^n \right\|_E^2$$

$$+ \frac{\Delta t}{2} \sum_{n=0}^{N-1} \left\| \sqrt{\delta} \boldsymbol{\eta}_h^{n+\frac{1}{2}} - \frac{1}{\sqrt{\delta}} \frac{\boldsymbol{v}_h^{n+1} - \boldsymbol{u}_h^n}{2} \right\|_E^2 \leq \exp \left( \frac{T\beta C_{inv}^2 \Delta t}{\rho_s h \Delta x^2 - \beta C_{inv}^2 \Delta t^2} \right)$$

$$\left( \frac{\rho_f}{2} \|\boldsymbol{u}_h^0\|_{L^2(\Omega)}^2 + \frac{\rho_s h}{2} \|\boldsymbol{u}_h^0\|_{L^2(\Gamma)}^2 + \frac{1}{2} \|\boldsymbol{\eta}_h^0\|_E^2 + \frac{\mu \Delta t}{2} \left\| \boldsymbol{D}(\boldsymbol{u}_h^0) \right\|_{L^2(\Omega)}^2 \right). \qquad \square$$

*Remark* 4.1. The stability result in Theorem 4.3 is achieved using Lemma 4.1, introducing the exponential function in the energy estimate. The reason that the Gronwall lemma is used is related to the second-order approximation of the fluid and structure subproblems, as well as the choice of test functions that allowed us the use of (3.13). Although theoretically this result may not be indicative of long-time stability, our numerical results show that the CNFSI scheme is stable and accurate when applied to realistic blood flow modeling. Similar estimates involving the Gronwall lemma are also obtained in the analysis of second-order splitting in [15].

**5. Error analysis.** To approximate the problem in space, we apply the Lagrangian finite elements of polynomial degree $k$ for all the variables, except for the

fluid pressure, for which we use elements of degree $s < k$. We assume that our finite element spaces satisfy the usual approximation properties and that the fluid velocity-pressure spaces satisfy the discrete inf-sup condition.

Let $a \lesssim (\gtrsim) b$ denote that there exists a positive constant $C$, independent of the mesh size $\Delta x$ and the time step size $\Delta t$, such that $a \leq (\geq) Cb$. We introduce the following time discrete norms:

$$(5.1) \qquad \|\boldsymbol{\varphi}\|_{L^2(0,T;X)} = \left( \Delta t \sum_{n=0}^{N-1} \|\boldsymbol{\varphi}^{n+1}\|_X^2 \right)^{\frac{1}{2}}, \quad \|\boldsymbol{\varphi}\|_{L^\infty(0,T;X)} = \max_{0 \leq n \leq N} \|\boldsymbol{\varphi}^n\|_X,$$

where $X \in \{H^k(\Omega), H^k(\Gamma), E\}$. Note that they are equivalent to the continuous norms since we use piecewise constant approximations in time. Furthermore, the following inequality holds:

$$(5.2) \qquad \Delta t \sum_{n=1}^{N-1} \|d_t \boldsymbol{\varphi}\|_X^2 \lesssim \|\partial_t \boldsymbol{\varphi}\|_{L^2(0,T;X)}^2 \,.$$

Let $I_h$ be the Lagrangian interpolation operator onto $V_h^s$. As in [8, 15], we introduce a Stokes-like projection operator $(S_h, P_h) : V^f \to V_h^f \times Q_h$, defined for all $\boldsymbol{u} \in V^f$ by

$$(5.3) \qquad (S_h \boldsymbol{u}, P_h \boldsymbol{u}) \in V_h^f \times Q_h,$$

$$(5.4) \qquad (S_h \boldsymbol{u})|_\Gamma = I_h(\boldsymbol{u}|_\Gamma),$$

$$(5.5) \qquad a_f(S_h \boldsymbol{u}, \boldsymbol{\varphi}_h) - b(P_h \boldsymbol{u}, \boldsymbol{\varphi}_h) = a_f(\boldsymbol{u}, \boldsymbol{\varphi}_h) \quad \forall \boldsymbol{\varphi}_h \in V_h^f \text{ such that } \boldsymbol{\varphi}_h|_\Gamma = 0,$$

$$(5.6) \qquad b(q, S_h \boldsymbol{u}) = 0 \quad \forall q \in Q_h.$$

Projection operators $S_h$ and $I_h$ satisfy the following approximation properties (see [15, Theorem B.5] and [13]):

$$\|\boldsymbol{D}(\boldsymbol{u} - S_h \boldsymbol{u})\|_{L^2(\Omega)} \lesssim \Delta x^k \|\boldsymbol{u}\|_{H^{k+1}(\Omega)} \quad \forall \boldsymbol{u} \in V^f,$$

$$\|\boldsymbol{v} - I_h \boldsymbol{v}\|_{L^2(\Gamma)} + \Delta x \|\boldsymbol{v} - I_h \boldsymbol{v}\|_{H^1(\Gamma)} \lesssim \Delta x^{k+1} \|\boldsymbol{v}\|_{H^{k+1}(\Gamma)} \quad \forall \boldsymbol{v} \in V^s.$$

Let $R_h$ be the Ritz projector onto $V_h^s$ such that for all $\boldsymbol{\eta} \in V^s$

$$(5.7) \qquad a_e(\boldsymbol{\eta} - R_h \boldsymbol{\eta}, \boldsymbol{\zeta}_h) = 0 \quad \forall \boldsymbol{\zeta}_h \in V_h^s.$$

Then, the finite element theory for Ritz projections [13] gives

$$\|\boldsymbol{\eta} - R_h \boldsymbol{\eta}\|_E \lesssim \Delta x^k \|\boldsymbol{\eta}\|_{H^{k+1}(\Gamma)} \quad \forall \boldsymbol{\eta} \in V^s.$$

Let $\Pi_h$ be a projection operator onto $Q_h^f$ such that

$$\|p - \Pi_h p\|_{L^2(\Omega)} \lesssim \Delta x^{s+1} \|p\|_{H^{s+1}(\Omega)} \quad \forall p \in Q^f.$$

The following two lemmas will be used in the convergence analysis.

LEMMA 5.1 (interpolation errors). *The following inequalities hold:*

$$\Delta t \sum_{n=0}^{N-1} \left\| \boldsymbol{\sigma}(\boldsymbol{u}^{n+\frac{1}{2}} - S_h \boldsymbol{u}^{n+\frac{1}{2}}, p^{n+\frac{1}{2}} - \Pi_h p^{n+\frac{1}{2}}) \boldsymbol{n} \right\|_{L^2(\Gamma)}^2$$

$$\lesssim \Delta x^{2s+2} \|p\|_{L^2(0,T;H^{s+1}(\Gamma))}^2 + \Delta x^{2k} \mu \|\boldsymbol{u}\|_{L^2(0,T;H^{k+1}(\Gamma))}^2,$$

$$\Delta t \sum_{n=0}^{N-1} \left\| \boldsymbol{\sigma}(\boldsymbol{u}^{n+\frac{1}{2}} - S_h \boldsymbol{u}^{n+\frac{1}{2}}, p^{n+\frac{1}{2}} - \Pi_h p^{n+\frac{1}{2}}) \boldsymbol{n} \right.$$

$$\left. - \boldsymbol{\sigma}(\boldsymbol{u}^{n-\frac{1}{2}} - S_h \boldsymbol{u}^{n+\frac{1}{2}}, p^{n-\frac{1}{2}} - \Pi_h p^{n+\frac{1}{2}}) \right\|_E^2$$

$$\lesssim \beta C_{inv}^2 \left( \Delta x^{2s} \|p\|_{L^2(0,T;H^{s+1}(\Gamma))}^2 + \Delta x^{2k-2} \|\boldsymbol{u}\|_{L^2(0,T;H^{k+1}(\Gamma))}^2 \right).$$

LEMMA 5.2 (consistency errors). *The following inequalities hold for $X \in \{L^2(\Omega), L^2(\Gamma), E\}$:*

$$\Delta t \sum_{n=1}^{N-1} \left\| \boldsymbol{\varphi}^{n+\frac{1}{2}} - \boldsymbol{\varphi}^{n-\frac{1}{2}} \right\|_X^2 \lesssim \Delta t^2 \|\partial_t \boldsymbol{\varphi}\|_{L^2(0,T;X)}^2,$$

$$\Delta t \sum_{n=1}^{N-1} \left\| \partial_t \boldsymbol{\varphi}^{n+\frac{1}{2}} - d_t \boldsymbol{\varphi}^{n+1} \right\|_X^2 \lesssim \Delta t^4 \|\partial_{ttt} \boldsymbol{\varphi}\|_{L^2(0,T;X)}^2,$$

$$\Delta t \sum_{n=1}^{N-1} \left\| \boldsymbol{\sigma}\left(\boldsymbol{u}^{n+\frac{1}{2}}, p^{n+\frac{1}{2}}\right) \boldsymbol{n} - \boldsymbol{\sigma}\left(\boldsymbol{u}^{n-\frac{1}{2}}, p^{n-\frac{1}{2}}\right) \boldsymbol{n} \right\|_E^2 \lesssim \Delta t^2 \|\partial_t \boldsymbol{\sigma} \boldsymbol{n}\|_{L^2(0,T;H^1(\Gamma))}^2.$$

In order to study convergence, we rewrite the CNFSI scheme (3.5)–(3.12) by using (3.10) to express $\boldsymbol{v}_h$ in terms of $\boldsymbol{u}_h$, resulting in the following problem:

(5.8)
$$\rho_f d_t \boldsymbol{u}_h^{n+1} = \nabla \cdot \boldsymbol{\sigma}\left(\boldsymbol{u}_h^{n+\frac{1}{2}}, p_h^{n+\frac{1}{2}}\right) \qquad\qquad \text{in } \Omega,$$

(5.9)
$$\nabla \cdot \boldsymbol{u}_h^{n+1} = 0 \qquad\qquad \text{in } \Omega,$$

(5.10)
$$\rho_s h d_t \boldsymbol{u}_h^{n+1} + \mathcal{L}_e \boldsymbol{\eta}_h^{n+\frac{1}{2}} = -\boldsymbol{\sigma}\left(\boldsymbol{u}_h^{n+\frac{1}{2}}, p_h^{n+\frac{1}{2}}\right) \boldsymbol{n} \qquad\qquad \text{on } \Gamma,$$

(5.11)
$$d_t \boldsymbol{\eta}_h^{n+1} - \boldsymbol{u}_h^{n+\frac{1}{2}} - \frac{\Delta t}{2\rho_s h}\left(\boldsymbol{\sigma}\left(\boldsymbol{u}_h^{n+\frac{1}{2}}, p_h^{n+\frac{1}{2}}\right) \boldsymbol{n} - \boldsymbol{\sigma}\left(\boldsymbol{u}_h^{n-\frac{1}{2}}, p_h^{n-\frac{1}{2}}\right) \boldsymbol{n}\right) = 0 \quad \text{on } \Gamma,$$

with boundary conditions (3.7), (3.11), and (3.12). Subtracting (5.8)–(5.11) from (2.10)–(2.13) evaluated at $t = t^{n+\frac{1}{2}}$ and defining $\boldsymbol{u}^{-\frac{1}{2}} = 0, p^{-\frac{1}{2}} = 0$, we obtain the following error equations:

(5.12)
$$\rho_f \left(d_t \boldsymbol{u}^{n+\frac{1}{2}} - d_t \boldsymbol{u}_h^{n+1}\right) = \nabla \cdot \boldsymbol{\sigma}\left(\boldsymbol{u}^{n+\frac{1}{2}} - \boldsymbol{u}_h^{n+\frac{1}{2}}, p^{n+\frac{1}{2}} - p_h^{n+\frac{1}{2}}\right)$$
$$+ \rho_f \left(d_t \boldsymbol{u}^{n+\frac{1}{2}} - \partial_t \boldsymbol{u}^{n+\frac{1}{2}}\right) \qquad\qquad \text{in } \Omega,$$

(5.13)
$$\nabla \cdot (\boldsymbol{u}^{n+\frac{1}{2}} - \boldsymbol{u}_h^{n+1}) = 0 \qquad\qquad \text{in } \Omega,$$

(5.14)
$$\rho_s h \left(d_t \boldsymbol{u}^{n+\frac{1}{2}} - d_t \boldsymbol{u}_h^{n+1}\right) + \mathcal{L}_e \left(\boldsymbol{\eta}^{n+\frac{1}{2}} - \boldsymbol{\eta}_h^{n+\frac{1}{2}}\right)$$
$$= -\boldsymbol{\sigma}\left(\boldsymbol{u}^{n+\frac{1}{2}} - \boldsymbol{u}_h^{n+\frac{1}{2}}, p^{n+\frac{1}{2}} - p_h^{n+\frac{1}{2}}\right) \boldsymbol{n} + \rho_s h \left(d_t \boldsymbol{u}^{n+\frac{1}{2}} - \partial_t \boldsymbol{u}^{n+\frac{1}{2}}\right) \qquad\qquad \text{on } \Gamma,$$

(5.15)

$$d_t\boldsymbol{\eta}^{n+\frac{1}{2}} - d_t\boldsymbol{\eta}_h^{n+1} - \left(\boldsymbol{u}^{n+\frac{1}{2}} - \boldsymbol{u}_h^{n+\frac{1}{2}}\right)$$

$$+ \frac{\Delta t}{2\rho_s h}\left(\boldsymbol{\sigma}\left(\boldsymbol{u}^{n+\frac{1}{2}} - \boldsymbol{u}_h^{n+\frac{1}{2}}, p^{n+\frac{1}{2}} - p_h^{n+\frac{1}{2}}\right)\boldsymbol{n} - \boldsymbol{\sigma}\left(\boldsymbol{u}^{n-\frac{1}{2}} - \boldsymbol{u}_h^{n-\frac{1}{2}}, p^{n-\frac{1}{2}} - p_h^{n-\frac{1}{2}}\right)\boldsymbol{n}\right)$$

$$= d_t\boldsymbol{\eta}^{n+\frac{1}{2}} - \partial_t\boldsymbol{\eta}^{n+\frac{1}{2}} + \frac{\Delta t}{2\rho_s h}\left(\boldsymbol{\sigma}\left(\boldsymbol{u}^{n+\frac{1}{2}}, p^{n+\frac{1}{2}}\right)\boldsymbol{n} - \boldsymbol{\sigma}\left(\boldsymbol{u}^{n-\frac{1}{2}}, p^{n-\frac{1}{2}}\right)\boldsymbol{n}\right) \quad \text{on } \Gamma,$$

with homogeneous Neumann conditions on $\Gamma_{in}$ and $\Gamma_{out}$.

We assume that the continuous solution satisfies the following assumptions:

$$\boldsymbol{u} \in H^1(0,T;H^{k+1}(\Omega)) \cap H^3(0,T;L^2(\Omega)), \quad \boldsymbol{u}|_\Gamma \in H^1(0,T;H^{k+1}(\Gamma)) \cap H^3(0,T;L^2(\Gamma)),$$

$$p \in L^2(0,T;H^{s+1}(\Omega)), \quad p|_\Gamma \in L^2(0,T;H^{s+1}(\Gamma)) \cap H^1(0,T;H^1(\Gamma)),$$

$$\boldsymbol{\eta} \in H^1(0,T;H^{k+1}(\Gamma)) \cap H^3(0,T;H^1(\Gamma)).$$

Furthermore, we define the functional spaces $V^m = \{\boldsymbol{\varphi} \in V^f | \ \boldsymbol{\varphi}|_\Gamma \in V^s\}$ and $V_h^m = \{\boldsymbol{\varphi} \in V_h^f | \ \boldsymbol{\varphi}|_\Gamma \in V_h^s\}$ and assume that the discrete fluid velocity belongs to $V_h^m$ and the continuous fluid velocity lives in the space $V^d = \{\boldsymbol{u} \in V^m | \ \nabla \cdot \boldsymbol{u} = 0\}$. The main result of this section is stated in the following theorem.

THEOREM 5.3. *Consider the finite element solution* $(\boldsymbol{u}_h, p_h, \boldsymbol{\eta}_h)$ *of* (5.8)–(5.11) *with initial data* $(\boldsymbol{u}_h^0, p_h^0, \boldsymbol{\eta}_h^0) = (S_h\boldsymbol{u}^0, \Pi_h p^0, R_h\boldsymbol{\eta}^0)$. *Assume that the CFL condition* (4.3) *holds and that*

$$\Delta t + \frac{\beta C_{inv}^2 \Delta t^2}{\rho_s h \Delta x^2} < \frac{1}{2}.$$

*Then, the following estimate holds:*

(5.16)

$$\frac{\rho_f}{2}\left\|\boldsymbol{u}^N - \boldsymbol{u}_h^N\right\|_{L^2(\Omega)}^2 + \frac{\rho_s h}{2}\left\|\boldsymbol{u}^N - \boldsymbol{u}_h^N\right\|_{L^2(\Gamma)}^2 + \frac{1}{2}\left\|\boldsymbol{\eta}^N - \boldsymbol{\eta}_h^N\right\|_E^2$$

$$+ \frac{\mu\Delta t}{2}\left\|D(\boldsymbol{u}^N - \boldsymbol{u}_h^N)\right\|_{L^2(\Omega)}^2 + \frac{\Delta t^2}{4\rho_s h}\left\|\boldsymbol{\sigma}(\boldsymbol{u}^{N-\frac{1}{2}} - \boldsymbol{u}_h^{N-\frac{1}{2}}, p^{N-\frac{1}{2}} - p_h^{N-\frac{1}{2}})\boldsymbol{n}\right\|_{L^2(\Gamma)}^2$$

$$+ 2\mu\Delta t\sum_{n=0}^{N-1}\|D(\boldsymbol{u}^{n+\frac{1}{2}} - \boldsymbol{u}_h^{n+\frac{1}{2}})\|_{L^2(\Omega)}^2 \lesssim \exp\left(\frac{T\max\{\frac{1}{2\Delta t}, 2\left(1 + \frac{\beta C_{inv}^2\Delta t}{\rho_s h\Delta x^2}\right)\}}{1 - \Delta t\max\{\frac{1}{2\Delta t}, 2\left(1 + \frac{\beta C_{inv}^2\Delta t}{\rho_s h\Delta x^2}\right)\}}\right)$$

$$\left(\Delta x^{2k}\mathcal{A}_1 + \Delta x^{2k+1}\mathcal{A}_2 + \Delta x^{2k+2}\mathcal{A}_3 + \Delta x^{2k+3}\mathcal{A}_4 + \Delta x^{2s+2}\mathcal{A}_5 + \Delta x^{2s+4}\mathcal{A}_6\right.$$

$$\left. + \Delta t^4\mathcal{A}_7 + \Delta t^5\mathcal{A}_8\right),$$

*where*

$$\mathcal{A}_1 = \rho_f\|\boldsymbol{u}\|_{L^\infty(0,T;H^{k+1}(\Omega))}^2 + \rho_f\|\partial_t\boldsymbol{u}\|_{L^2(0,T;H^{k+1}(\Omega))}^2 + \mu\|\boldsymbol{u}\|_{L^2(0,T;H^{k+1}(\Omega))}^2$$

$$+ \|\boldsymbol{\eta}\|_{L^\infty(0,T;H^{k+1}(\Gamma))}^2 + \|\boldsymbol{\eta}\|_{L^2(0,T;H^{k+1}(\Gamma))}^2$$

$$+ \|\partial_t\boldsymbol{\eta}\|_{L^2(0,T;H^{k+1}(\Gamma))}^2 + \left(1 + \frac{\beta C_{inv}^2\mu}{\rho_s^2 h^2}\right)\|\boldsymbol{u}\|_{L^2(0,T;H^{k+1}(\Gamma))}^2,$$

$$\mathcal{A}_2 = \mu\|\boldsymbol{u}\|_{L^\infty(0,T;H^{k+1}(\Omega))}^2,$$

$$\mathcal{A}_3 = (\rho_s h + \mu) \,\|\boldsymbol{u}\|^2_{L^\infty(0,T;H^{k+1}(\Gamma))} + \rho_s h \,\|\partial_t \boldsymbol{u}\|^2_{L^2(0,T;H^{k+1}(\Gamma))} + \frac{\mu}{\rho_s h} \,\|\boldsymbol{u}\|^2_{L^2(0,T;H^{k+1}(\Gamma))} \,,$$

$$\mathcal{A}_4 = \rho_s h \,\|\partial_t \boldsymbol{u}\|^2_{L^2(0,T;H^{k+1}(\Gamma))} \,,$$

$$\mathcal{A}_5 = \frac{C_k^2 d}{\mu} \,\|p\|^2_{L^2(0,T;H^{s+1}(\Omega))} + \frac{\beta C_{inv}^2}{\rho_s^2 h^2} \,\|p\|^2_{L^2(0,T;H^{s+1}(\Gamma))} \,,$$

$$\mathcal{A}_6 = \frac{1}{\rho_s h} \,\|p\|^2_{L^2(0,T;H^{s+1}(\Gamma))} + \|p\|^2_{L^\infty(0,T;H^{s+1}(\Gamma))} \,,$$

$$\mathcal{A}_7 = \rho_f \,\|\partial_{ttt}\boldsymbol{u}\|^2_{L^2(0,T;L^2(\Omega))} + \rho_s h \,\|\partial_{ttt}\boldsymbol{u}\|^2_{L^2(0,T;L^2(\Gamma))} + \|\partial_{ttt}\boldsymbol{\eta}\|^2_{L^2(0,T;H^1(\Gamma))}$$

$$+ \frac{1}{\rho_s^2 h^2} \,\|\partial_t \boldsymbol{\sigma}\,(\boldsymbol{u},p)\,\boldsymbol{n}\|^2_{L^2(0,T;H^1(\Gamma))} \,,$$

$$\mathcal{A}_8 = \rho_s h \,\|\partial_{ttt}\boldsymbol{u}\|^2_{L^2(0,T;L^2(\Gamma))} \,.$$

*Proof.* We split the error of the method as a sum of the approximation error $\theta_r^{n+1}$ and the truncation error $\delta_r^{n+1}$ for $r \in \{f,p,\eta\}$ as follows:

(5.17)
$$e_f^{n+1} = \boldsymbol{u}^{n+1} - \boldsymbol{u}_h^{n+1} = (\boldsymbol{u}^{n+1} - S_h \boldsymbol{u}^{n+1}) + (S_h \boldsymbol{u}^{n+1} - \boldsymbol{u}_h^{n+1}) = \boldsymbol{\theta}_f^{n+1} + \boldsymbol{\delta}_f^{n+1},$$

(5.18)
$$e_p^{n+1} = p^{n+1} - p_h^{n+1} = (p^{n+1} - \Pi_h p^{n+1}) + (\Pi_h p^{n+1} - p_h^{n+1}) = \theta_p^{n+1} + \delta_p^{n+1},$$

(5.19)
$$e_s^{n+1} = \boldsymbol{\eta}^{n+1} - \boldsymbol{\eta}_h^{n+1} = (\boldsymbol{\eta}^{n+1} - R_h \boldsymbol{\eta}^{n+1}) + (R_h \boldsymbol{\eta}^{n+1} - \boldsymbol{\eta}_h^{n+1}) = \boldsymbol{\theta}_\eta^{n+1} + \delta_\eta^{n+1}.$$

We substitute (5.17)–(5.19) into (5.12)–(5.15) and multiply (5.12) by $\Delta t \boldsymbol{\delta}_f^{n+1}$, (5.13) by $\Delta t \delta_p^{n+\frac{1}{2}}$, and (5.15) by $\Delta t \mathcal{L}_e(\boldsymbol{\eta}^{n+\frac{1}{2}} - \boldsymbol{\eta}_h^{n+\frac{1}{2}})$. Adding the equations, integrating by parts, and using (5.14) as a Robin boundary condition in (5.12), we get

(5.20)
$$\frac{\rho_f}{2}\left(\|\boldsymbol{\delta}_f^{n+1}\|^2_{L^2(\Omega)} - \|\boldsymbol{\delta}_f^n\|^2_{L^2(\Omega)} + \|\boldsymbol{\delta}_f^{n+1} - \boldsymbol{\delta}_f^n\|^2_{L^2(\Omega)}\right)$$

$$+ \frac{\mu\Delta t}{2}\left(\|D(\boldsymbol{\delta}_f^{n+1})\|^2_{L^2(\Omega)} - \|D(\boldsymbol{\delta}_f^n)\|^2_{L^2(\Omega)} + 4\|D(\boldsymbol{\delta}_f^{n+\frac{1}{2}})\|^2_{L^2(\Omega)}\right)$$

$$+ \frac{\rho_s h}{2}\left(\|\boldsymbol{\delta}_f^{n+1}\|^2_{L^2(\Gamma)} - \|\boldsymbol{\delta}_f^n\|^2_{L^2(\Gamma)} + \|\boldsymbol{\delta}_f^{n+1} - \boldsymbol{\delta}_f^n\|^2_{L^2(\Gamma)}\right)$$

$$+ a_e\left(\boldsymbol{\theta}_\eta^{n+\frac{1}{2}}, \boldsymbol{\delta}_f^{n+1}\right) - \Delta t\, b\left(\delta_p^{n+\frac{1}{2}}, \boldsymbol{\delta}_f^{n+1}\right) - \Delta t\, b\left(\delta_p^{n+\frac{1}{2}}, \boldsymbol{u}_h^{n+1}\right)$$

$$= \underbrace{-\Delta t\, a_e\left(\boldsymbol{\delta}_\eta^{n+\frac{1}{2}}, \boldsymbol{\delta}_f^{n+1}\right) - \Delta t \int_\Gamma d_t \boldsymbol{\delta}_\eta^{n+1} \cdot \mathcal{L}_e(\boldsymbol{\eta}^{n+\frac{1}{2}} - \boldsymbol{\eta}_h^{n+\frac{1}{2}}) dS + \Delta t \int_\Gamma \boldsymbol{\delta}_f^{n+\frac{1}{2}} \cdot \mathcal{L}_e(\boldsymbol{\eta}^{n+\frac{1}{2}} - \boldsymbol{\eta}_h^{n+\frac{1}{2}}) dS}_{T_1}$$

$$\underbrace{+ \frac{\Delta t^2}{2\rho_s h} \int_\Gamma \left(\boldsymbol{\sigma}\left(\boldsymbol{\delta}_f^{n+\frac{1}{2}}, \delta_p^{n+\frac{1}{2}}\right)\boldsymbol{n} - \boldsymbol{\sigma}\left(\boldsymbol{\delta}_f^{n-\frac{1}{2}}, \delta_p^{n-\frac{1}{2}}\right)\boldsymbol{n}\right) \cdot \mathcal{L}_e(\boldsymbol{\eta}^{n+\frac{1}{2}} - \boldsymbol{\eta}_h^{n+\frac{1}{2}}) dS}_{T_2}$$

$$- \rho_f \Delta t \int_\Omega d_t \boldsymbol{\theta}_f^{n+1} \cdot \boldsymbol{\delta}_f^{n+1} d\boldsymbol{x} - \Delta t\, a_f(\boldsymbol{\theta}_f^{n+\frac{1}{2}}, \boldsymbol{\delta}_f^{n+1}) + \Delta t\, b(\theta_p^{n+\frac{1}{2}}, \boldsymbol{\delta}_f^{n+1}) - \Delta t \rho_s h \int_\Gamma d_t \boldsymbol{\theta}_f^{n+1} \cdot \delta_f^{n+1} dS$$

$$- \Delta t \int_\Gamma d_t \boldsymbol{\theta}_\eta^{n+1} \cdot \mathcal{L}_e(\boldsymbol{\eta}^{n+\frac{1}{2}} - \boldsymbol{\eta}_h^{n+\frac{1}{2}}) dS + \Delta t \int_\Gamma \boldsymbol{\theta}_f^{n+\frac{1}{2}} \cdot \mathcal{L}_e(\boldsymbol{\eta}^{n+\frac{1}{2}} - \boldsymbol{\eta}_h^{n+\frac{1}{2}}) dS$$

$$+ \frac{\Delta t^2}{2\rho_s h} \int_\Gamma \left(\boldsymbol{\sigma}\left(\boldsymbol{\theta}_f^{n+\frac{1}{2}}, \theta_p^{n+\frac{1}{2}}\right)\boldsymbol{n} - \boldsymbol{\sigma}\left(\boldsymbol{\theta}_f^{n-\frac{1}{2}}, \theta_p^{n-\frac{1}{2}}\right)\boldsymbol{n}\right) \cdot \mathcal{L}_e(\boldsymbol{\eta}^{n+\frac{1}{2}} - \boldsymbol{\eta}_h^{n+\frac{1}{2}}) dS + \Delta t \left(\mathcal{R}^f + \mathcal{R}^e\right),$$

where

$$\mathcal{R}^f = \rho_f \int_\Omega \left( d_t \boldsymbol{u}^{n+1} - \partial_t \boldsymbol{u}^{n+\frac{1}{2}} \right) \cdot \boldsymbol{\delta}_f^{n+1} d\boldsymbol{x} + \rho_s h \int_\Gamma (d_t \boldsymbol{u}^{n+1} - \partial_t \boldsymbol{u}^{n+\frac{1}{2}}) \cdot \boldsymbol{\delta}_f^{n+1} dS,$$

$$\mathcal{R}^e = \int_\Gamma \left( d_t \boldsymbol{\eta}^{n+1} - \partial_t \boldsymbol{\eta}^{n+\frac{1}{2}} \right) \cdot \mathcal{L}_e(\boldsymbol{\eta}^{n+\frac{1}{2}} - \boldsymbol{\eta}_h^{n+\frac{1}{2}}) dS$$
$$- \frac{\Delta t}{2\rho_s h} \int_\Gamma \left( \boldsymbol{\sigma}\left( \boldsymbol{u}^{n+\frac{1}{2}}, p^{n+\frac{1}{2}} \right) \boldsymbol{n} - \boldsymbol{\sigma}\left( \boldsymbol{u}^{n-\frac{1}{2}}, p^{n-\frac{1}{2}} \right) \boldsymbol{n} \right) \cdot \mathcal{L}_e(\boldsymbol{\eta}^{n+\frac{1}{2}} - \boldsymbol{\eta}_h^{n+\frac{1}{2}}) dS.$$

Since $\boldsymbol{\delta}_f^{n+\frac{1}{2}}|_\Gamma \in V_h^s$, by the Ritz projection operator property (5.7) we have $a_e(\boldsymbol{\theta}_\eta^{n+\frac{1}{2}}, \boldsymbol{\delta}_f^{n+\frac{1}{2}}) = 0$. Furthermore, using the Stokes projection property (5.6), the pressure terms on the left-hand side vanish

$$-\Delta t b(\delta_p^{n+\frac{1}{2}}, \boldsymbol{\delta}_f^{n+1}) - \Delta t b(\delta_p^{n+\frac{1}{2}}, \boldsymbol{u}_h^{n+1}) = -\Delta t b(\delta_p^{n+\frac{1}{2}}, S_h \boldsymbol{u}^{n+1}) = 0.$$

Applying (2.15), adding and subtracting $R_h \boldsymbol{\eta}^{n+\frac{1}{2}}$, and using the Ritz projection operator property (5.7), term $T_1$ simplifies as follows:

$$T_1 = -\Delta t a_e \left( \boldsymbol{\delta}_\eta^{n+\frac{1}{2}}, \delta_f^{n+1} \right) - \Delta t a_e \left( \boldsymbol{\eta}^{n+\frac{1}{2}} - R_h \boldsymbol{\eta}^{n+\frac{1}{2}} + R_h \boldsymbol{\eta}^{n+\frac{1}{2}} - \boldsymbol{\eta}_h^{n+\frac{1}{2}}, d_t \boldsymbol{\delta}_\eta^{n+1} - \boldsymbol{\delta}_f^{n+\frac{1}{2}} \right)$$
$$= -\Delta t a_e \left( \boldsymbol{\delta}_\eta^{n+\frac{1}{2}}, \delta_f^{n+1} \right) - \Delta t a_e \left( \boldsymbol{\delta}_\eta^{n+\frac{1}{2}}, d_t \boldsymbol{\delta}_\eta^{n+1} - \boldsymbol{\delta}_f^{n+\frac{1}{2}} \right)$$
$$= -\frac{1}{2} \left\| \boldsymbol{\delta}_\eta^{n+1} \right\|_E^2 + \frac{1}{2} \left\| \boldsymbol{\delta}_\eta^n \right\|_E^2 - \Delta t a_e \left( \boldsymbol{\delta}_\eta^{n+\frac{1}{2}}, \frac{\boldsymbol{\delta}_f^{n+1} - \boldsymbol{\delta}_f^n}{2} \right).$$

Using the Cauchy–Schwarz inequality, Young's inequality with $\delta > 0$, and (4.1), we have

$$\Delta t a_e \left( \boldsymbol{\delta}_\eta^{n+\frac{1}{2}}, \frac{\boldsymbol{\delta}_f^{n+1} - \boldsymbol{\delta}_f^n}{2} \right) \leq \frac{\delta \Delta t}{2} \left\| \boldsymbol{\delta}_\eta^{n+\frac{1}{2}} \right\|_E^2 + \frac{\Delta t}{2\delta} \left\| \frac{\boldsymbol{\delta}_f^{n+1} - \boldsymbol{\delta}_f^n}{2} \right\|_E^2$$
$$\leq \frac{\delta \Delta t}{2} \left\| \boldsymbol{\delta}_\eta^{n+\frac{1}{2}} \right\|_E^2 + \frac{\beta C_{inv}^2 \Delta t}{8\delta \Delta x^2} \left\| \boldsymbol{\delta}_f^{n+1} - \boldsymbol{\delta}_f^n \right\|_{L^2(\Gamma)}^2.$$

Let $\delta = \dfrac{3\beta C_{inv}^2 \Delta t}{4\rho_s h \Delta x^2}$. Thus,

$$T_1 \leq -\frac{1}{2} \left\| \boldsymbol{\delta}_\eta^{n+1} \right\|_E^2 + \frac{1}{2} \left\| \boldsymbol{\delta}_\eta^n \right\|_E^2 + \frac{3\beta C_{inv}^2 \Delta t^2}{16\rho_s h \Delta x^2} \left\| \boldsymbol{\delta}_\eta^{n+1} \right\|_E^2$$
$$\text{(5.21)} \qquad + \frac{3\beta C_{inv}^2 \Delta t^2}{16\rho_s h \Delta x^2} \left\| \boldsymbol{\delta}_\eta^n \right\|_E^2 + \frac{\rho_s h}{6} \left\| \boldsymbol{\delta}_f^{n+1} - \boldsymbol{\delta}_f^n \right\|_{L^2(\Gamma)}^2.$$

To estimate integral $T_2$, we first note that using (5.17)–(5.18) in (5.14) gives

$$\mathcal{L}_e(\boldsymbol{\eta}^{n+\frac{1}{2}} - \boldsymbol{\eta}_h^{n+\frac{1}{2}}) = -\boldsymbol{\sigma}\left( \boldsymbol{\theta}_f^{n+\frac{1}{2}} + \boldsymbol{\delta}_f^{n+\frac{1}{2}}, \theta_p^{n+\frac{1}{2}} + \delta_p^{n+\frac{1}{2}} \right) \boldsymbol{n}$$
$$\text{(5.22)} \qquad - \rho_s h \left( d_t \boldsymbol{\theta}_f^{n+1} + d_t \boldsymbol{\delta}_f^{n+1} + \partial_t \boldsymbol{u}^{n+\frac{1}{2}} - d_t \boldsymbol{u}^{n+1} \right).$$

Using (5.22), term $T_2$ now becomes

$$
\begin{aligned}
T_2 = & -\frac{\Delta t^2}{4\rho_s h}\left(\left\|\boldsymbol{\sigma}\left(\boldsymbol{\delta}_f^{n+\frac{1}{2}},\delta_p^{n+\frac{1}{2}}\right)\boldsymbol{n}\right\|_{L^2(\Gamma)}^2 - \left\|\boldsymbol{\sigma}\left(\boldsymbol{\delta}_f^{n-\frac{1}{2}},\delta_p^{n-\frac{1}{2}}\right)\boldsymbol{n}\right\|_{L^2(\Gamma)}^2\right) \\
& -\frac{\Delta t^2}{4\rho_s h}\left\|\boldsymbol{\sigma}\left(\boldsymbol{\delta}_f^{n+\frac{1}{2}},\delta_p^{n+\frac{1}{2}}\right)\boldsymbol{n}-\boldsymbol{\sigma}\left(\boldsymbol{\delta}_f^{n-\frac{1}{2}},\delta_p^{n-\frac{1}{2}}\right)\boldsymbol{n}\right\|_{L^2(\Gamma)}^2 \\
& -\frac{\Delta t^2}{2\rho_s h}\int_\Gamma\left(\boldsymbol{\sigma}\left(\boldsymbol{\delta}_f^{n+\frac{1}{2}},\delta_p^{n+\frac{1}{2}}\right)\boldsymbol{n}-\boldsymbol{\sigma}\left(\boldsymbol{\delta}_f^{n-\frac{1}{2}},\delta_p^{n-\frac{1}{2}}\right)\boldsymbol{n}\right)\cdot\boldsymbol{\sigma}\left(\boldsymbol{\theta}_f^{n+\frac{1}{2}},\theta_p^{n+\frac{1}{2}}\right)\boldsymbol{n}dS \\
& -\frac{\Delta t^2}{2}\int_\Gamma\left(\boldsymbol{\sigma}\left(\boldsymbol{\delta}_f^{n+\frac{1}{2}},\delta_p^{n+\frac{1}{2}}\right)\boldsymbol{n}-\boldsymbol{\sigma}\left(\boldsymbol{\delta}_f^{n-\frac{1}{2}},\delta_p^{n-\frac{1}{2}}\right)\boldsymbol{n}\right) \\
& \cdot\left(d_t\boldsymbol{\theta}_f^{n+1}+d_t\boldsymbol{\delta}_f^{n+1}+\partial_t\boldsymbol{u}^{n+\frac{1}{2}}-d_t\boldsymbol{u}^{n+1}\right)dS.
\end{aligned}
$$

Applying Cauchy–Schwarz and Young's inequalities, we have

(5.23)
$$
\begin{aligned}
T_2 \leq & -\frac{\Delta t^2}{4\rho_s h}\left(\left\|\boldsymbol{\sigma}\left(\boldsymbol{\delta}_f^{n+\frac{1}{2}},\delta_p^{n+\frac{1}{2}}\right)\boldsymbol{n}\right\|_{L^2(\Gamma)}^2 - \left\|\boldsymbol{\sigma}\left(\boldsymbol{\delta}_f^{n-\frac{1}{2}},\delta_p^{n-\frac{1}{2}}\right)\boldsymbol{n}\right\|_{L^2(\Gamma)}^2\right) \\
& -\frac{\Delta t^2}{64\rho_s h}\left\|\boldsymbol{\sigma}\left(\boldsymbol{\delta}_f^{n+\frac{1}{2}},\delta_p^{n+\frac{1}{2}}\right)\boldsymbol{n}-\boldsymbol{\sigma}\left(\boldsymbol{\delta}_f^{n-\frac{1}{2}},\delta_p^{n-\frac{1}{2}}\right)\boldsymbol{n}\right\|_{L^2(\Gamma)}^2+\frac{2\rho_s h}{7}\left\|\boldsymbol{\delta}_f^{n+1}-\boldsymbol{\delta}_f^n\right\|_{L^2(\Gamma)}^2 \\
& +\frac{12\Delta t^2}{\rho_s h}\left\|\boldsymbol{\sigma}\left(\boldsymbol{\theta}_f^{n+\frac{1}{2}},\theta_p^{n+\frac{1}{2}}\right)\boldsymbol{n}\right\|_{L^2(\Gamma)}^2+12\Delta t^2\rho_s h\left\|d_t\boldsymbol{\theta}_f^{n+1}\right\|_{L^2(\Gamma)}^2 \\
& +12\Delta t^2\rho_s h\left\|\partial_t\boldsymbol{u}^{n+\frac{1}{2}}-d_t\boldsymbol{u}^{n+1}\right\|_{L^2(\Gamma)}^2.
\end{aligned}
$$

Substituting (5.21) and (5.23) into (5.20), summing from $0\leq n\leq N-1$, and taking into account assumptions on the initial data, we get

(5.24)
$$
\begin{aligned}
& \frac{\rho_f}{2}\left\|\boldsymbol{\delta}_f^N\right\|_{L^2(\Omega)}^2 + \frac{\rho_s h}{2}\left\|\boldsymbol{\delta}_f^N\right\|_{L^2(\Gamma)}^2 + \frac{1}{2}\left\|\boldsymbol{\delta}_\eta^N\right\|_E^2 + \frac{\mu\Delta t}{2}\left\|D(\boldsymbol{\delta}_f^N)\right\|_{L^2(\Omega)}^2 + \frac{\Delta t^2}{4\rho_s h}\left\|\boldsymbol{\sigma}\left(\boldsymbol{\delta}_f^{N-\frac{1}{2}},\delta_p^{N-\frac{1}{2}}\right)\boldsymbol{n}\right\|_{L^2(\Gamma)}^2 \\
& +\frac{\rho_f}{2}\sum_{n=0}^{N-1}\left\|\boldsymbol{\delta}_f^{n+1}-\boldsymbol{\delta}_f^n\right\|_{L^2(\Omega)}^2 + \frac{\rho_s h}{21}\sum_{n=0}^{N-1}\left\|\boldsymbol{\delta}_f^{n+1}-\boldsymbol{\delta}_f^n\right\|_{L^2(\Gamma)}^2 + 2\mu\Delta t\sum_{n=0}^{N-1}\|D(\boldsymbol{\delta}_f^{n+\frac{1}{2}})\|_{L^2(\Omega)}^2 \\
& +\frac{\Delta t^2}{64\rho_s h}\sum_{n=0}^{N-1}\left\|\boldsymbol{\sigma}\left(\boldsymbol{\delta}_f^{n+\frac{1}{2}},\delta_p^{n+\frac{1}{2}}\right)\boldsymbol{n}-\boldsymbol{\sigma}\left(\boldsymbol{\delta}_f^{n-\frac{1}{2}},\delta_p^{n-\frac{1}{2}}\right)\boldsymbol{n}\right\|_{L^2(\Gamma)}^2 \\
& \lesssim \underbrace{-\Delta t\sum_{n=0}^{N-1}\left(\int_\Omega\rho_f d_t\boldsymbol{\theta}_f^{n+1}\cdot\boldsymbol{\delta}_f^{n+1}dx + a_f\left(\boldsymbol{\theta}_f^{n+\frac{1}{2}},\boldsymbol{\delta}_f^{n+1}\right) - b\left(\theta_p^{n+\frac{1}{2}},\boldsymbol{\delta}_f^{n+1}\right) + \rho_s h\int_\Gamma d_t\boldsymbol{\theta}_f^{n+1}\cdot\boldsymbol{\delta}_f^{n+1}dS\right)}_{T_3} \\
& \underbrace{-\Delta t\sum_{n=0}^{N-1}\left(\int_\Gamma d_t\boldsymbol{\theta}_\eta^{n+1}\cdot\mathcal{L}_e\left(\boldsymbol{\eta}^{n+\frac{1}{2}}-\boldsymbol{\eta}_h^{n+\frac{1}{2}}\right)dS - \int_\Gamma\boldsymbol{\theta}_f^{n+\frac{1}{2}}\cdot\mathcal{L}_e\left(\boldsymbol{\eta}^{n+\frac{1}{2}}-\boldsymbol{\eta}_h^{n+\frac{1}{2}}\right)dS\right)}_{T_4} \\
& \underbrace{+\frac{\Delta t^2}{2\rho_s h}\sum_{n=0}^{N-1}\int_\Gamma\left(\boldsymbol{\sigma}\left(\boldsymbol{\theta}_f^{n+\frac{1}{2}},\theta_p^{n+\frac{1}{2}}\right)\boldsymbol{n}-\boldsymbol{\sigma}\left(\boldsymbol{\theta}_f^{n-\frac{1}{2}},\theta_p^{n-\frac{1}{2}}\right)\boldsymbol{n}\right)\cdot\mathcal{L}_e\left(\boldsymbol{\eta}^{n+\frac{1}{2}}-\boldsymbol{\eta}_h^{n+\frac{1}{2}}\right)dS}_{T_5} \\
& +\frac{\Delta t^2}{\rho_s h}\sum_{n=0}^{N-1}\left\|\boldsymbol{\sigma}\left(\boldsymbol{\theta}_f^{n+\frac{1}{2}},\theta_p^{n+\frac{1}{2}}\right)\boldsymbol{n}\right\|_{L^2(\Gamma)}^2 + \Delta t^2\sum_{n=0}^{N-1}\rho_s h\left\|d_t\boldsymbol{\theta}_f^{n+1}\right\|_{L^2(\Gamma)}^2 \\
& +\Delta t^2\rho_s h\sum_{n=0}^{N-1}\left\|\partial_t\boldsymbol{u}^{n+\frac{1}{2}}-d_t\boldsymbol{u}^{n+1}\right\|_{L^2(\Gamma)}^2 + \Delta t\sum_{n=0}^{N-1}\left(\mathcal{R}^f+\mathcal{R}^e\right) + \sum_{n=0}^N\frac{\beta C_{inv}^2\Delta t^2}{\rho_s h\Delta x^2}\left\|\boldsymbol{\delta}_\eta^n\right\|_E^2.
\end{aligned}
$$

To estimate $T_3$, we employ the Cauchy–Schwarz, Young's, and Korn's inequalities, as well as $\|\nabla \cdot \boldsymbol{\delta}_f^{n+1}\| \leq \sqrt{d}\|\nabla \boldsymbol{\delta}_f^{n+1}\|$, as follows:

(5.25)

$$
T_3 \leq \Delta t \sum_{n=1}^{N-1} \left( \rho_f \left\| d_t \boldsymbol{\theta}_f^{n+1} \right\|_{L^2(\Omega)}^2 + \frac{\rho_f}{4} \left\| \boldsymbol{\delta}_f^{n+1} \right\|_{L^2(\Omega)}^2 \right.
$$
$$
\left. + \rho_s h \left\| d_t \boldsymbol{\theta}_f^{n+1} \right\|_{L^2(\Gamma)}^2 + \frac{\rho_s h}{4} \left\| \boldsymbol{\delta}_f^{n+1} \right\|_{L^2(\Gamma)}^2 \right)
$$
$$
+ \Delta t \sum_{n=1}^{N-1} \left( 8\mu \left\| D(\boldsymbol{\theta}_f^{n+\frac{1}{2}}) \right\|_{L^2(\Omega)}^2 + \frac{2C_k^2 d}{\mu} \left\| \theta_p^{n+\frac{1}{2}} \right\|_{L^2(\Omega)}^2 + \frac{\mu}{4} \left\| D(\boldsymbol{\delta}_f^{n+1}) \right\|_{L^2(\Omega)}^2 \right).
$$

Using (2.15) and (5.19), term $T_4$ can be written as follows:

$$
T_4 = -\Delta t \sum_{n=1}^{N-1} \left( a_e \left( \boldsymbol{\delta}_\eta^{n+\frac{1}{2}} + \boldsymbol{\theta}_\eta^{n+\frac{1}{2}}, d_t \boldsymbol{\theta}_\eta^{n+1} \right) - a_e \left( \boldsymbol{\delta}_\eta^{n+\frac{1}{2}} + \boldsymbol{\theta}_\eta^{n+\frac{1}{2}}, \boldsymbol{\theta}_f^{n+\frac{1}{2}} \right) \right).
$$

Using the Ritz projection property (5.7) and Cauchy–Schwarz and Young's inequalities, we have

$$
T_4 = -\Delta t \sum_{n=1}^{N-1} \left( a_e \left( \boldsymbol{\theta}_\eta^{n+\frac{1}{2}}, d_t \boldsymbol{\theta}_\eta^{n+1} \right) - a_e \left( \boldsymbol{\delta}_\eta^{n+\frac{1}{2}}, \boldsymbol{\theta}_f^{n+\frac{1}{2}} \right) - a_e \left( \boldsymbol{\theta}_\eta^{n+\frac{1}{2}}, \boldsymbol{\theta}_f^{n+\frac{1}{2}} \right) \right)
$$
$$
(5.26) \quad \leq \Delta t \sum_{n=1}^{N-1} \left( \left\| \boldsymbol{\theta}_\eta^{n+\frac{1}{2}} \right\|_E^2 + \frac{1}{2} \left\| d_t \boldsymbol{\theta}_\eta^{n+1} \right\|_E^2 + \frac{1}{4} \left\| \boldsymbol{\delta}_\eta^{n+\frac{1}{2}} \right\|_E^2 + \frac{3}{2} \left\| \boldsymbol{\theta}_f^{n+\frac{1}{2}} \right\|_E^2 \right).
$$

In a similar way, we estimate term $T_5$:

$$
T_5 = \frac{\Delta t^2}{2\rho_s h} \sum_{n=1}^{N-1} a_e \left( \boldsymbol{\delta}_\eta^{n+\frac{1}{2}} + \boldsymbol{\theta}_\eta^{n+\frac{1}{2}}, \boldsymbol{\sigma} \left( \boldsymbol{\theta}_f^{n+\frac{1}{2}}, \theta_p^{n+\frac{1}{2}} \right) \boldsymbol{n} - \boldsymbol{\sigma} \left( \boldsymbol{\theta}_f^{n-\frac{1}{2}}, \theta_p^{n-\frac{1}{2}} \right) \boldsymbol{n} \right) dS
$$
$$
\leq \Delta t \sum_{n=1}^{N-1} \left( \frac{1}{4} \left\| \boldsymbol{\delta}_\eta^{n+\frac{1}{2}} \right\|_E^2 + \frac{1}{4} \left\| \boldsymbol{\theta}_\eta^{n+\frac{1}{2}} \right\|_E^2 + \frac{\Delta t^2}{2\rho_s^2 h^2} \right.
$$
$$
(5.27) \qquad\qquad \left. \left\| \boldsymbol{\sigma} \left( \boldsymbol{\theta}_f^{n+\frac{1}{2}}, \theta_p^{n+\frac{1}{2}} \right) \boldsymbol{n} - \boldsymbol{\sigma} \left( \boldsymbol{\theta}_f^{n-\frac{1}{2}}, \theta_p^{n-\frac{1}{2}} \right) \boldsymbol{n} \right\|_E^2 \right).
$$

Finally, we estimate the consistency error terms as follows. Applying the Cauchy–Schwarz and Young's inequalities, we have

$$
\Delta t \sum_{n=1}^{N-1} \mathcal{R}^f \leq \Delta t \sum_{n=1}^{N-1} \left( \rho_f \left\| d_t \boldsymbol{u}^{n+1} - \partial_t \boldsymbol{u}^{n+\frac{1}{2}} \right\|_{L^2(\Omega)}^2 + \frac{\rho_f}{4} \left\| \boldsymbol{\delta}_f^{n+1} \right\|_{L^2(\Omega)}^2 \right)
$$
$$
(5.28) \qquad + \Delta t \sum_{n=1}^{N-1} \left( \rho_s h \left\| d_t \boldsymbol{u}^{n+1} - \partial_t \boldsymbol{u}^{n+\frac{1}{2}} \right\|_{L^2(\Gamma)}^2 + \frac{\rho_s h}{4} \left\| \boldsymbol{\delta}_f^{n+1} \right\|_{L^2(\Gamma)}^2 \right).
$$

Using (2.15) and (5.19), then applying the Cauchy–Schwarz and Young's inequalities, we have

$$\Delta t \sum_{n=1}^{N-1} \mathcal{R}^e = \Delta t \sum_{n=1}^{N-1} a_e \left( \boldsymbol{\theta}_\eta^{n+\frac{1}{2}} + \boldsymbol{\delta}_\eta^{n+\frac{1}{2}}, d_t \boldsymbol{\eta}^{n+1} - \partial_t \boldsymbol{\eta}^{n+\frac{1}{2}} \right)$$

$$- \frac{\Delta t^2}{2\rho_s h} \sum_{n=1}^{N-1} a_e \left( \boldsymbol{\theta}_\eta^{n+\frac{1}{2}} + \boldsymbol{\delta}_\eta^{n+\frac{1}{2}}, \left( \boldsymbol{\sigma} \left( \boldsymbol{u}^{n+\frac{1}{2}}, p^{n+\frac{1}{2}} \right) \boldsymbol{n} - \boldsymbol{\sigma} \left( \boldsymbol{u}^{n-\frac{1}{2}}, p^{n-\frac{1}{2}} \right) \boldsymbol{n} \right) \right)$$

$$\leq \Delta t \sum_{n=1}^{N-1} \left( \frac{1}{2} \left\| \boldsymbol{\theta}_\eta^{n+\frac{1}{2}} \right\|_E^2 + \frac{1}{2} \left\| \boldsymbol{\delta}_\eta^{n+\frac{1}{2}} \right\|_E^2 + 2 \left\| d_t \boldsymbol{\eta}^{n+1} - \partial_t \boldsymbol{\eta}^{n+\frac{1}{2}} \right\|_E^2 \right)$$

$$(5.29) \qquad + \frac{\Delta t^3}{2\rho_s^2 h^2} \sum_{n=1}^{N-1} \left\| \left( \boldsymbol{\sigma} \left( \boldsymbol{u}^{n+\frac{1}{2}}, p^{n+\frac{1}{2}} \right) \boldsymbol{n} - \boldsymbol{\sigma} \left( \boldsymbol{u}^{n-\frac{1}{2}}, p^{n-\frac{1}{2}} \right) \right) \boldsymbol{n} \right\|_E^2 .$$

Substituting (5.25)–(5.29) into the error equation (5.24), we obtain

$$\frac{\rho_f}{2} \left\| \boldsymbol{\delta}_f^N \right\|_{L^2(\Omega)}^2 + \frac{\rho_s h}{2} \left\| \boldsymbol{\delta}_f^N \right\|_{L^2(\Gamma)}^2 + \frac{1}{2} \left\| \boldsymbol{\delta}_\eta^N \right\|_E^2 + \frac{\mu \Delta t}{2} \left\| D(\boldsymbol{\delta}_f^N) \right\|_{L^2(\Omega)}^2$$

$$+ \frac{\Delta t^2}{4\rho_s h} \left\| \boldsymbol{\sigma} \left( \boldsymbol{\delta}_f^{N-\frac{1}{2}}, \delta_p^{N-\frac{1}{2}} \right) \boldsymbol{n} \right\|_{L^2(\Gamma)}^2 + \frac{\rho_f}{2} \sum_{n=0}^{N-1} \left\| \boldsymbol{\delta}_f^{n+1} - \boldsymbol{\delta}_f^n \right\|_{L^2(\Omega)}^2$$

$$+ \frac{\rho_s h}{21} \sum_{n=0}^{N-1} \left\| \boldsymbol{\delta}_f^{n+1} - \boldsymbol{\delta}_f^n \right\|_{L^2(\Gamma)}^2 + 2\mu \Delta t \sum_{n=0}^{N-1} \| D(\boldsymbol{\delta}_f^{n+\frac{1}{2}}) \|_{L^2(\Omega)}^2$$

$$+ \frac{\Delta t^2}{64\rho_s h} \sum_{n=0}^{N-1} \left\| \boldsymbol{\sigma} \left( \boldsymbol{\delta}_f^{n+\frac{1}{2}}, \delta_p^{n+\frac{1}{2}} \right) \boldsymbol{n} - \boldsymbol{\sigma} \left( \boldsymbol{\delta}_f^{n-\frac{1}{2}}, \delta_p^{n-\frac{1}{2}} \right) \boldsymbol{n} \right\|_{L^2(\Gamma)}^2$$

$$\lesssim \Delta t \sum_{n=0}^{N-1} \left( \rho_f \left\| d_t \boldsymbol{\theta}_f^{n+1} \right\|_{L^2(\Omega)}^2 + \rho_s h (1 + \Delta t) \left\| d_t \boldsymbol{\theta}_f^{n+1} \right\|_{L^2(\Gamma)}^2 + \mu \left\| D(\boldsymbol{\theta}_f^{n+\frac{1}{2}}) \right\|_{L^2(\Omega)}^2 \right.$$

$$+ \frac{C_k^2 d}{\mu} \left\| \theta_p^{n+\frac{1}{2}} \right\|_{L^2(\Omega)}^2 + \left\| \boldsymbol{\theta}_\eta^{n+\frac{1}{2}} \right\|_E^2 + \left\| d_t \boldsymbol{\theta}_\eta^{n+1} \right\|_E^2 + \left\| \boldsymbol{\theta}_f^{n+\frac{1}{2}} \right\|_E^2$$

$$+ \frac{\Delta t^2}{\rho_s^2 h^2} \left\| \boldsymbol{\sigma} \left( \boldsymbol{\theta}_f^{n+\frac{1}{2}}, \theta_p^{n+\frac{1}{2}} \right) \boldsymbol{n} - \boldsymbol{\sigma} \left( \boldsymbol{\theta}_f^{n-\frac{1}{2}}, \theta_p^{n-\frac{1}{2}} \right) \boldsymbol{n} \right\|_E^2 + \frac{\Delta t^2}{\rho_s h} \left\| \boldsymbol{\sigma} \left( \boldsymbol{\theta}_f^{n+\frac{1}{2}}, \theta_p^{n+\frac{1}{2}} \right) \boldsymbol{n} \right\|_{L^2(\Gamma)}^2 \right)$$

$$+ \Delta t \sum_{n=0}^{N-1} \left( \rho_f \left\| d_t \boldsymbol{u}^{n+1} - \partial_t \boldsymbol{u}^{n+\frac{1}{2}} \right\|_{L^2(\Omega)}^2 + \rho_s h (1 + \Delta t) \left\| d_t \boldsymbol{u}^{n+1} - \partial_t \boldsymbol{u}^{n+\frac{1}{2}} \right\|_{L^2(\Gamma)}^2 \right.$$

$$+ \left\| d_t \boldsymbol{\eta}^{n+1} - \partial_t \boldsymbol{\eta}^{n+\frac{1}{2}} \right\|_E^2 + \frac{\Delta t^2}{\rho_s^2 h^2} \left\| \left( \boldsymbol{\sigma} \left( \boldsymbol{u}^{n+\frac{1}{2}}, p^{n+\frac{1}{2}} \right) \boldsymbol{n} - \boldsymbol{\sigma} \left( \boldsymbol{u}^{n-\frac{1}{2}}, p^{n-\frac{1}{2}} \right) \right) \boldsymbol{n} \right\|_E^2 \right)$$

$$+ \Delta t \sum_{n=0}^{N} \left( \frac{\rho_f}{2} \| \boldsymbol{\delta}_f^n \|_{L^2(\Omega)}^2 + \frac{\rho_s h}{2} \| \boldsymbol{\delta}_f^n \|_{L^2(\Gamma)}^2 + \frac{\mu}{4} \| D(\boldsymbol{\delta}_f^n) \|_{L^2(\Omega)}^2 + \left( 1 + \frac{\beta C_{inv}^2 \Delta t}{\rho_s h \Delta x^2} \right) \| \boldsymbol{\delta}_\eta^n \|_E^2 \right).$$

Using (5.2), estimates in Lemmas 5.1 and 5.2 and taking into account the CFL condition (4.3) we have

$$\frac{\rho_f}{2} \| \boldsymbol{\delta}_f^N \|_{L^2(\Omega)}^2 + \frac{\rho_s h}{2} \| \boldsymbol{\delta}_f^N \|_{L^2(\Gamma)}^2 + \frac{1}{2} \| \boldsymbol{\delta}_\eta^N \|_E^2 + \frac{\mu \Delta t}{2} \| D(\boldsymbol{\delta}_f^N) \|_{L^2(\Omega)}^2$$

$$+ \frac{\Delta t^2}{4\rho_s h} \left\| \boldsymbol{\sigma} \left( \boldsymbol{\delta}_f^{N-\frac{1}{2}}, \delta_p^{N-\frac{1}{2}} \right) \boldsymbol{n} \right\|_{L^2(\Gamma)}^2 + 2\mu \Delta t \sum_{n=0}^{N-1} \| D(\boldsymbol{\delta}_f^{n+\frac{1}{2}}) \|_{L^2(\Omega)}^2$$

$$\lesssim \Delta x^{2k} \left( \rho_f \| \partial_t \boldsymbol{u} \|_{L^2(0,T;H^{k+1}(\Omega))}^2 + \rho_s h \Delta x^2 (1 + \Delta x) \| \partial_t \boldsymbol{u} \|_{L^2(0,T;H^{k+1}(\Gamma))}^2 \right.$$

$$+ \mu \|\boldsymbol{u}\|^2_{L^2(0,T;H^{k+1}(\Omega))} + \left( \frac{\mu \Delta x^2}{\rho_s h} + 1 + \frac{\beta C_{inv}^2 \mu}{\rho_s^2 h^2} \right) \|\boldsymbol{u}\|^2_{L^2(0,T;H^{k+1}(\Gamma))}$$

$$+ \|\partial_t \boldsymbol{\eta}\|^2_{L^2(0,T;H^{k+1}(\Gamma))} + \|\boldsymbol{\eta}\|^2_{L^2(0,T;H^{k+1}(\Gamma))} \bigg)$$

$$+ \Delta x^{2s+2} \left( \frac{C_k^2 d}{\mu} \|p\|^2_{L^2(0,T;H^{s+1}(\Omega))} + \left( \frac{\beta C_{inv}^2}{\rho_s^2 h^2} + \frac{\Delta x^2}{\rho_s h} \right) \|p\|^2_{L^2(0,T;H^{s+1}(\Gamma))} \right)$$

$$+ \Delta t^4 \Big( \rho_f \|\partial_{ttt} \boldsymbol{u}\|^2_{L^2(0,T;L^2(\Omega))} + \rho_s h \ (1 + \Delta t) \|\partial_{ttt} \boldsymbol{u}\|^2_{L^2(0,T;L^2(\Gamma))} + \|\partial_{ttt} \boldsymbol{\eta}\|^2_{L^2(0,T;E)}$$

$$+ \frac{1}{\rho_s^2 h^2} \|\partial_t \boldsymbol{\sigma}(\boldsymbol{u}, p)\,\boldsymbol{n}\|^2_{L^2(0,T;H^1(\Gamma))} \Big) + \Delta t \sum_{n=0}^{N} \left( \frac{\rho_f}{2} \|\boldsymbol{\delta}_f^n\|^2_{L^2(\Omega)} + \frac{\rho_s h}{2} \|\boldsymbol{\delta}_f^n\|^2_{L^2(\Gamma)} \right.$$

$$+ \frac{\mu}{4} \|D(\boldsymbol{\delta}_f^n)\|^2_{L^2(\Omega)} + \left( 1 + \frac{\beta C_{inv}^2 \Delta t}{\rho_s h \Delta x^2} \right) \|\boldsymbol{\delta}_\eta^n\|^2_E \bigg). \qquad \square$$

The final estimate follows by applying the triangle inequality and Lemma 4.1 with

$$\gamma_n = \max \left\{ \frac{1}{2\Delta t}, 2 \left( 1 + \frac{\beta C_{inv}^2 \Delta t}{\rho_s h \Delta x^2} \right) \right\}.$$

**6. Numerical examples.** In this section we test the accuracy and stability of the CNFSI numerical scheme on two examples. First we consider a classical benchmark problem used to test FSI solvers [18, 9, 1, 6, 10, 8]. Using this example, we study the convergence of scheme (3.5)–(3.12) in two spatial dimensions in Example 1. Then, to demonstrate applicability of the CNFSI scheme to realistic blood flow simulations on a three-dimensional example, we model blood flow in a common carotid artery under physiological conditions in Example 2.

**6.1. Example 1: Benchmark problem for FSI with elastic structure.** To verify the convergence rates, we consider the benchmark problem used to verify FSI solvers in [10, 8, 15]. In this example, we assume that the fluid domain is a rectangle $\Omega = [0,5] \times [0, 0.5]$. The top boundary corresponds to the fluid-structure interface, while symmetry conditions are prescribed at the bottom boundary. The flow is driven by the time-dependent pressure data

$$p_{in}(t) = \begin{cases} \frac{p_{max}}{2} \left( 1 - \cos \left( \frac{2\pi t}{t_{max}} \right) \right) & \text{it } t \le t_{max}, \\ 0 & \text{it } t > t_{max}, \end{cases} \qquad p_{out}(t) = 0 \quad \forall t \in (0, T),$$

where $p_{max} = 1.3333 \cdot 10^4$ dyne/cm$^2$ and $t_{max} = 3$ ms. The problem is solved over the time interval $[0, 14]$ ms. To discretize the problem in space, we use the $\mathbb{P}_1$ bubble–$\mathbb{P}_1$ elements for the velocity and pressure and $\mathbb{P}_1$ elements for displacement. The values of the parameters used in this example are given in Table 1.

To model the fluid flow, we used the Stokes equations. For the structure displacement, we consider a thin, elastic structure described by a generalized string model with the assumption of zero axial displacement:

$$\boldsymbol{\eta} = (0, \eta_y)^T, \quad \mathcal{L}_S \boldsymbol{\eta} = (0, C_0 \eta_y - C_1 \partial_{xx} \eta_y)^T$$

(6.1) $$\text{with } C_0 = \frac{Eh}{R^2(1 - \sigma^2)} \text{ and } C_1 = \frac{Eh}{2(1 + \sigma)},$$

where $E$ is the Young's modulus and $\sigma$ is Poisson's ratio. In this case, parameter $\beta$ that appears in (2.17) can be estimated as $\beta = 4 \cdot 10^5$. Using a uniform computational

| Parameter | Value | Parameter | Value |
|---|---|---|---|
| Radius $R$ (cm) | 0.5 | Wall thickness $h$ (cm) | 0.1 |
| Length $L$ (cm) | 5 | Poisson's ratio $\sigma$ | 0.5 |
| Fluid viscosity $\mu$ (g/(cm s)) | 0.035 | Young's mod. $E(\text{dyne/cm}^2)$ | $0.75 \cdot 10^6$ |
| Fluid density $\rho_f$ (g/cm$^3$) | 1 | Wall density $\rho_s$(g/cm$^3$) | 1.1 |
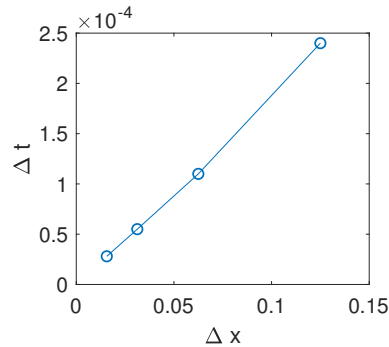


FIG. 2. *Relation between $\Delta x$ and $\Delta t$ which gave rise to a stable solution. Proportionality constant is $1.9 \cdot 10^{-3}$.*

mesh and the results from [24], we can estimate that $C_{inv} = 16.7$. Hence, in this test example the stability condition (4.3) gives

$$(6.2) \qquad \Delta t \leq 3.14 \cdot 10^{-5} \Delta x.$$

The sharpness of this condition was investigated numerically. Figure 2 shows the relation between $\Delta x$ and $\Delta t$ which gave rise to a stable solution. The proportionality constant in this case is $1.9 \cdot 10^{-3}$, which is less restrictive than the prediction (6.2) obtained from theory.

In order to verify the time convergence estimates from Theorem 5.3, we generate a reference solution using a monolithic scheme (2.18) with high grid resolution ($\Delta t = 10^{-6}, \Delta x = 0.0063$). To test the partitioned scheme, we refine in space and time at the same rate. In particular, we use

$$(\Delta t, \Delta x) \in \left\{ \left( \frac{10^{-4}}{2^k}, \frac{6.25 \cdot 10^{-1}}{2^k} \right) \right\}_{k=0}^{3}.$$

Due to the short simulation time ($T = 0.016$ s), the largest time step typically used in this benchmark problem is $\mathcal{O}(5 \cdot 10^{-4})$ s. We note that due to the stability condition (4.3), the largest time step we could use to obtain stable results is $\Delta t = 10^{-4}$. Figure 3 shows relative error for the fluid velocity in $L^2$-norm (left) and for the structure displacement in $\| \cdot \|_E$ norm (right) obtained at $T = 8$ ms. Indeed, the error estimates (5.16) yield the observed time-convergence rates.

**6.2. Example 2: Blood flow in common carotid artery.** The carotid arteries are major blood vessels in the neck that supply blood to the brain, neck, and face. To demonstrate performance of our scheme in realistic applications, we simulate blood flow in a common carotid artery under physiological conditions in a three-dimensional case. We also compare our results to the ones obtained using a monolithic scheme.
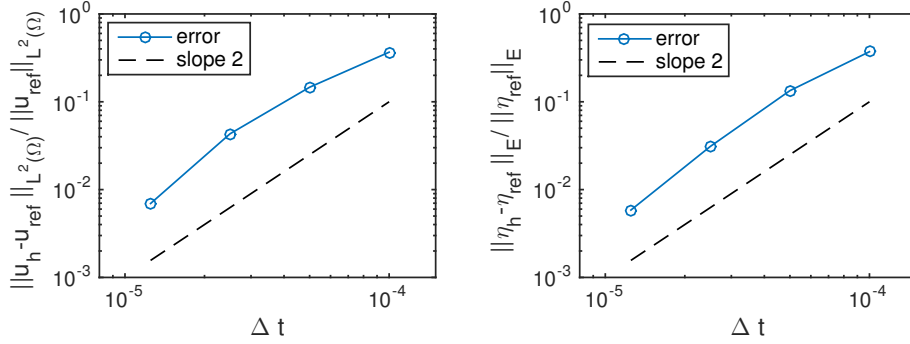
FIG. 3. *Time convergence obtained at $t = 8$ ms. Left: Relative error for fluid velocity in the $L^2$-norm. Right: Relative error for the structure displacement in the $\| \cdot \|_E$ norm.*
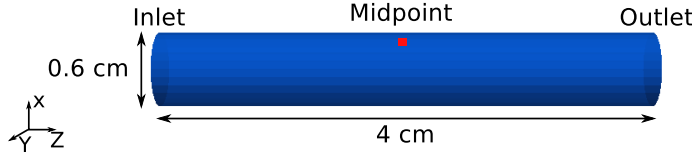


FIG. 4. *Computational three-dimensional domain used in Example 2.*

We model the common carotid artery as a straight cylinder of length 4 cm and radius 0.3 cm; see Figure 4. Similarly as in [25], at the fluid inlet section we prescribe a fully developed time-dependent axial velocity, while a pressure waveform is imposed at the outlet. In particular, we impose the following conditions:

$$(6.3) \qquad \boldsymbol{u} = \left( 0, 0, u_D(t) \frac{R^2 - r}{R^2} \right) \quad \text{on } \Gamma_{in}^f \quad \text{and} \quad \boldsymbol{\sigma} \boldsymbol{n} = -p_{out}(t) \boldsymbol{n} \quad \text{on } \Gamma_{out}^f,$$

where $r$ is the radial distance from the origin and $u_D(t)$ and $p_{out}(t)$ are shown in Figure 5.

The blood is modeled using the Navier–Stokes equation for a viscous, incompressible fluid. The thin structure model used in this example is a linear membrane model [17, 16, 14], given in the weak form as

$$(6.4)$$
$$\rho_s h \int_\Gamma \frac{\partial^2 \boldsymbol{\eta}}{\partial t^2} \cdot \boldsymbol{\zeta} dS + \underbrace{\int_\Gamma D_1 \boldsymbol{\eta} \cdot \boldsymbol{\zeta} dS + \int_\Gamma D_2 \frac{\partial \boldsymbol{\eta}}{\partial t} \cdot \boldsymbol{\zeta} dS + h \int_\Gamma \boldsymbol{\Pi}_\gamma(\boldsymbol{\eta}) : \nabla_\gamma \boldsymbol{\zeta} dS}_{a_e(\boldsymbol{\eta}, \boldsymbol{\zeta})} = \int_{\Gamma^s} \boldsymbol{f} \cdot \boldsymbol{\zeta} dS,$$

where $\boldsymbol{\eta} = (\eta_x, \eta_y, \eta_z)$ denotes the structure displacement. For a linearly elastic, isotropic structure

$$(6.5) \qquad \boldsymbol{\Pi}_\gamma(\boldsymbol{\eta}) = \frac{E}{1 + \sigma^2} \frac{\nabla_\gamma \boldsymbol{\eta} + \nabla_\gamma^T \boldsymbol{\eta}}{2} + \frac{E\sigma}{1 - \sigma^2} \nabla_\gamma \cdot \boldsymbol{\eta},$$

where $\nabla_\gamma(\cdot)$ denotes the surface gradient, which can be computed as [14, 7]

$$\nabla_\gamma(\boldsymbol{\eta}) = \nabla \boldsymbol{\eta}(\boldsymbol{I} - \boldsymbol{n} \otimes \boldsymbol{n}),$$
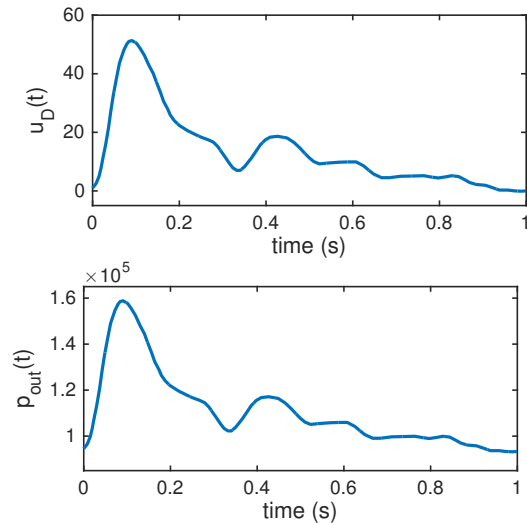
FIG. 5. *Boundary conditions for the fluid domain. Left: inlet velocity. Right: outlet pressure.*

TABLE 2
*Geometry, fluid, and structure parameters used in Example 2.*

| Parameter | Value | Parameter | Value |
|-----------|-------|-----------|-------|
| Radius $R$ (cm) | 0.3 | Wall thickness $h$ (cm) | 0.06 |
| Length $L$ (cm) | 4 | Poisson's ratio $\sigma$ | 0.5 |
| Fluid viscosity $\mu$ (g/(cm s)) | 0.04 | Young's mod. $E(\text{dyne/cm}^2)$ | $2.6 \cdot 10^6$ |
| Fluid density $\rho_f$ (g/cm$^3$) | 1 | Coefficient $D_1(\text{dyne/cm}^3)$ | $6 \cdot 10^5$ |
| Wall density $\rho_s$(g/cm$^3$) | 1.1 | Coefficient $D_2(\text{dyne s/cm}^3)$ | $2 \cdot 10^5$ |

where the symbol $\otimes$ denotes the tensor product and $\boldsymbol{I}$ is the identity operator. The co-efficients $E$ and $\sigma$ are the Young's modulus and the Poisson's ratio for the membrane, respectively. Terms multiplied by $D_1$ and $D_2$ in (6.4) take into account the constraining effects of the external tissue. Values of the parameters used in this example are given in Table 2.

The fluid mesh used in this example consists of 8181 vertices and 41280 tetrahedral elements, while the structure mesh consists of 2268 vertices and 4480 triangles. We used $\mathbb{P}_1$ bubble $-\mathbb{P}_1$ elements for the velocity and pressure and $\mathbb{P}_1$ elements for displacement. All initial conditions are set to zero. Even though the results are stable for a larger time step, $\Delta t = 10^{-4}$ is used in numerical simulations because that is the value needed to establish time step independence. The numerical simulations were performed for final time $T = 4$ s. The periodic regime was obtained after three cardiac cycles. To demonstrate that the periodic regime was established, the structure displacement over four cycles at the midpoint of the structure domain is shown in Figure 6. We note that the solution is axially symmetric, and the midpoint is chosen to be (0.3, 0, 2), shown in Figure 4. Similar results are obtained for the fluid velocity and pressure, i.e., the periodic regime is established after three cycles.

Using the same parameter setting, we performed numerical simulations using a monolithic scheme. Time step independence was established using $\Delta t = 5 \cdot 10^{-4}$. As with using the partitioned approach, periodic solutions are obtained after three cycles. Figure 7 shows a comparison of the results obtained using a monolithic scheme
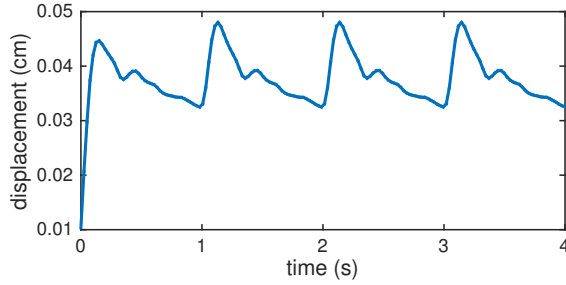
FIG. 6. *Structure displacement at the midpoint of the domain. After three cardiac cycles, the periodic regime is established.*
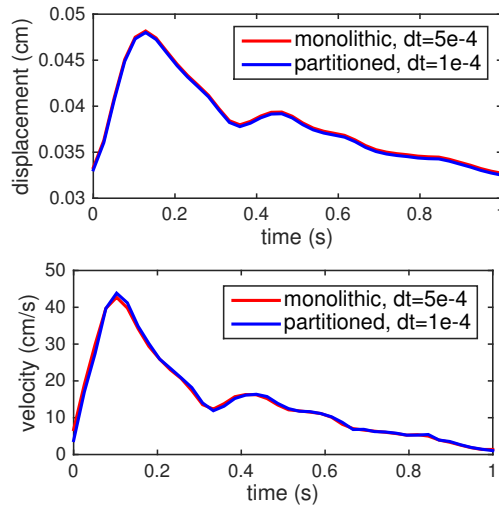


FIG. 7. *Comparison of the results obtained using the CNFSI scheme and a monolithic scheme. Left: structure displacement. Right: fluid velocity.*

and our scheme after the periodic regime was obtained. The left panel shows a comparison of the structure displacement at the midpoint of the structure domain $(0.5, 0, 2)$ and the right panel shows a comparison of the fluid velocity at the center of domain $(0,0,2)$. In both cases, the relative error between the solution obtained with a monolithic scheme and the CNFSI scheme is smaller than 1%. Although the partitioned scheme required a smaller time step than the monolithic scheme, the subproblems in the partitioned scheme are better conditioned than the monolithic scheme. More precisely, the stiffness matrices associated with the fluid and structure subproblems in the CNFSI scheme have a condition number of the order $\mathcal{O}(10^5)$, while the condition number of the stiffness matrix in the monolithic scheme is $\mathcal{O}(10^{10})$.

**7. Conclusions.** We present a partitioned, loosely coupled scheme for the interaction between a viscous, incompressible fluid and a thin, elastic structure. The time discretization is based on the Crank–Nicolson discretization method, and the discretization in space is performed using the finite element method. Using energy estimates, we show that the presented scheme is stable under a CFL condition. However, this condition is independent of the ratio between fluid and structure densities

and hence the scheme is not affected by the instabilities related to the added mass effect. Using a priori error analysis, we show that the scheme is second-order accurate in time and optimally accurate in space.

The energy of the system in the stability estimates is bounded by an exponential function due to the use of the Gronwall lemma. However, long time stability is demonstrated in the numerical results. The numerical examples include a benchmark problem used to verify the rates of convergence and a realistic study of blood flow in a common carotid artery. Our scheme is shown to be stable under physiological conditions related to blood flow and comparable in accuracy to a monolithic scheme. As expected, to achieve the same accuracy as the monolithic scheme, a smaller time step was needed. However, the proposed partitioned scheme requires the solution of smaller subproblems, without the use of preconditioners. Possible extensions of this work include nonlinear solids and thick structure models.

## REFERENCES

[1] S. BADIA, F. NOBILE, AND C. VERGARA, *Fluid-structure partitioned procedures based on Robin transmission conditions*, J. Comput. Phys., 227 (2008), pp. 7027–7051.

[2] S. BADIA, F. NOBILE, AND C. VERGARA, *Robin-Robin preconditioned Krylov methods for fluid-structure interaction problems*, Comput. Methods Appl. Mech. Engrg., 198 (2009), pp. 2768–2784.

[3] H. BAEK AND G. KARNIADAKIS, *A convergence study of a new partitioned fluid–structure interaction algorithm based on fictitious mass and damping*, J. Comput. Phys., 231 (2012), pp. 629–652.

[4] J. BANKS, W. HENSHAW, AND D. SCHWENDEMAN, *An analysis of a new stable partitioned algorithm for FSI problems. Part* I: *Incompressible flow and elastic solids*, J. Comput. Phys., 269 (2014), pp. 108–137.

[5] J. BANKS, W. HENSHAW, AND D. SCHWENDEMAN, *An analysis of a new stable partitioned algorithm for FSI problems. Part* II: *Incompressible flow and structural shells*, J. Comput. Phys., 268 (2014), pp. 399–416.

[6] A. BARKER AND X. CAI, *Scalable parallel methods for monolithic coupling in fluid-structure interaction with application to blood flow modeling*, J. Comput. Phys., 229 (2010), pp. 642–659.

[7] A. BONITO, R. NOCHETTO, AND M. PAULETTI, *Dynamics of biomembranes: Effect of the bulk fluid*, Math. Model. Nat. Phenom., 6 (2011), pp. 25–43.

[8] M. BUKAC AND B. MUHA, *Stability and convergence analysis of the extensions of the kinematically coupled scheme for the fluid-structure interaction*, SIAM J. Numer. Anal., 54 (2016), pp. 3032–3061.

[9] M. BUKAČ, I. YOTOV, AND P. ZUNINO, *An operator splitting approach for the interaction between a fluid and a multilayered poroelastic structure*, Numer. Methods Partial Differential Equations, 31 (2015), pp. 1054–1100.

[10] E. BURMAN AND M. FERNÁNDEZ, *Stabilization of explicit coupling in fluid-structure interaction involving fluid incompressibility*, Comput. Methods Appl. Mech. Engrg., 198 (2009), pp. 766–784.

[11] E. BURMAN AND M. FERNÁNDEZ, *An unfitted Nitsche method for incompressible fluid-structure interaction using overlapping meshes*, Comput. Methods Appl. Mech. Engrg., 279 (2014), pp. 497–514.

[12] P. CAUSIN, J. GERBEAU, AND F. NOBILE, *Added-mass effect in the design of partitioned algorithms for fluid-structure problems*, Comput. Methods Appl. Mech. Engrg., 194 (2005), pp. 4506–4527.

[13] P. CIARLET, *The Finite Element Method for Elliptic Problems*, Vol. 4, North-Holland, Amsterdam, 1978.

[14] C. COLCIAGO, S. DEPARIS, AND A. QUARTERONI, *Comparisons between reduced order models and full 3D models for fluid–structure interaction problems in haemodynamics*, J. Comput. Appl. Math., 265 (2014), pp. 120–138.

[15] M. FERNÁNDEZ, *Incremental displacement-correction schemes for incompressible fluid-structure interaction: Stability and convergence analysis*, Numer. Math., 123 (2013), pp. 21–65.

[16] A. Figueroa, S. Baek, C. Taylor, and J. Humphrey, *A computational framework for fluid–solid-growth modeling in cardiovascular simulations*, Comput. Methods Appl. Mech. Engrg., 198 (2009), pp. 3583–3602.

[17] C. Figueroa, I. Vignon-Clementel, K. Jansen, T. Hughes, and C. Taylor, *A coupled momentum method for modeling blood flow in three-dimensional deformable arteries*, Comput. Methods Appl. Mech. Engrg., 195 (2006), pp. 5685–5706.

[18] L. Formaggia, J. Gerbeau, F. Nobile, and A. Quarteroni, *On the coupling of 3D and 1D Navier-Stokes equations for flow problems in compliant vessels*, Comput. Methods Appl. Mech. Engrg., 191 (2001), pp. 561–582.

[19] J. Heywood and R. Rannacher, *Finite-element approximation of the nonstationary Navier–Stokes problem. Part IV: Error analysis for second-order time discretization*, SIAM J. Numer. Anal., 27 (1990), pp. 353–384.

[20] A. Hundertmark-Zaušková, M. Lukáčová-Medvid'ová, and G. Rusnáková, *Fluid-structure interaction for shear-dependent non-Newtonian fluids*, in Topics in Mathematical Modeling and Analysis, Jindřich Nečas Cent. Math. Model. Lect. Notes 7, Matfyzpress, Prague, 2012, pp. 109–158.

[21] M. Lukáčová-Medvidová, G. Rusnáková, and A. Hundertmark-Zaušková, *Kinematic splitting algorithm for fluid–structure interaction in hemodynamics*, Comput. Methods Appl. Mech. Engrg., 265 (2013), pp. 83–106.

[22] B. Muha and S. Čanić, *Existence of a weak solution to a nonlinear fluid–structure interaction problem modeling the flow of an incompressible, viscous fluid in a cylinder with deformable walls*, Arch. Ration. Mech. Anal., 207 (2013), pp. 919–968.

[23] F. Nobile and C. Vergara, *An effective fluid-structure interaction formulation for vascular dynamics by generalized Robin conditions*, SIAM J. Sci. Comput., 30 (2008), pp. 731–763.

[24] S. Özisik, B. Rivière, and T. Warburton, *On the Constants in Inverse Inequalities in L2*, Technical report TR10-19, Rice University, 2010.

[25] Z. Wang, N. Wood, and X. Xu, *A viscoelastic fluid–structure interaction model for carotid arteries under pulsatile flow*, Int. J. Numer. Methods Biomed. Eng., 31 (2015).

[26] Y. Yu, H. Baek, and G. Karniadakis, *Generalized fictitious methods for fluid–structure interactions: Analysis and simulations*, J. Comput. Phys., 245 (2013), pp. 317–346.